Search for the Optimal Design of a Supercritical-CO2 Brayton Power Cycle from a Superstructure-Based Approach Implemented in a Commercial Simulation Software

Qiao Zhao, Mounir Mecheri, Thibaut Neveux, Romain Privat, Jean-Noël Jaubert, Yann Le Moullec

energies

MDPI

Article

Search for the Optimal Design of a Supercritical-CO_2 Brayton Power Cycle from a Superstructure-Based Approach Implemented in a Commercial Simulation Software

Qiao Zhao [1,2], Mounir Mecheri [2], Thibaut Neveux [2], Romain Privat [1], Jean-Noël Jaubert [1,*] and Yann Le Moullec [2]

[1] École Nationale Supérieure des Industries Chimiques, Laboratoire Réactions et Génie des Procédés (UMR CNRS 7274), Université de Lorraine, 1 Rue Grandville, 54000 Nancy, France; qiao.zhao@axens.net (Q.Z.); romain.privat@univ-lorraine.fr (R.P.)

[2] EDF R&D Chatou, 6 Quai Watier, 78400 Chatou, France; mounir.mecheri@edf.fr (M.M.); thibaut.neveux@edf.fr (T.N.); yann.le-moullec@edf.fr (Y.L.M.)

* Correspondence: jean-noel.jaubert@univ-lorraine.fr

Abstract: Improving the efficiency and flexibility of fossil-fired power plants remains a current and challenging issue. In that regard, supercritical CO_2 Brayton cycles offer promising potential. This paper aims to apply a process synthesis approach to the design of a closed Brayton cycle using supercritical CO_2 as a working fluid with a coal furnace as a heat source. The general methodology presented here for designing closed power cycles includes the construction of a superstructure containing all relevant possible cycle layouts, the formulation of the cycle-synthesis problem as a mathematical optimization problem, and its solution using an appropriate algorithm. This study was conducted with the help of a process simulation commercial software (PROSIM) and using the Mixed-Integer Distributed Ant Colony Optimization (MIDACO) as a commercial optimization algorithm. This work highlights the limits of a purely technical optimization approach that would ignore the economical layer. The optimal structure obtained regarding Levelized Cost Of Electricity (LCOE) minimization is a configuration with one reheat of the supercritical CO_2 in the boiler, two recuperators, and one recompression loop around the low-temperature recuperator; it is associated with a cycle efficiency of 49.35 % and a 10% reduction in the LCOE in comparison to the optimal case found through energy optimization under typical design heuristics constraints.

Keywords: design optimization; S-CO_2 cycle; superstructure

Citation: Zhao, Q.; Mecheri, M.; Neveux, T.; Privat, R.; Jaubert, J.-N.; Le Moullec, Y. Search for the Optimal Design of a Supercritical-CO_2 Brayton Power Cycle from a Superstructure-Based Approach Implemented in a Commercial Simulation Software. *Energies* **2023**, *16*, 5470. https://doi.org/10.3390/en16145470

Academic Editor: Francesco Frusteri

Received: 25 June 2023
Revised: 7 July 2023
Accepted: 11 July 2023
Published: 19 July 2023

1. Introduction

In order to limit the negative impact of power generation from fossil fuels and nevertheless meet the growing demand for cheap and reliable electricity, power producers have been encouraged to improve the efficiency of their power plants in which the thermal efficiency of the power cycle has the highest impact. As an illustration, the Directive (EU) 2018/2002 of the European Parliament on energy efficiency states that "*all AEuropean countries are required to use energy more efficiently throughout the full energy chain, including energy generation, transmission, distribution and end-use, . . .*". In addition, renewable energy power generation is beginning to take a significant share of the power generation mix and is often replacing fossil-fired plants. Most of these new renewable plants are of the intermittent type and require proper backup capacity from the grid—backup that is given mostly by fossil-fired plants. For that reason, the transition toward power generation based exclusively on renewable energy sources exclusively will require decades of research, development, and investment. In the medium term, this transition will necessitate an increased need for the flexibility of these fossil-fired plants (startup time, minimal maintainability, efficiency at a low load factor). Then, this highest flexibility will allow the highest share of

renewable generation. In the coming years, the proportion of fossil-fuel-based systems will certainly decrease in favor of renewable-energy-based systems, but both types of systems will continue to coexist for a long time, especially in newly industrialized and developing countries. For all these reasons, improving the efficiency and flexibility of fossil-fired power plants remains, more than ever, a current and challenging issue. In that regard, supercritical carbon dioxide (S-CO_2) Brayton cycles offer promising potential.

1.1. S-CO_2 Brayton Cycles for Fossil-Fired Power Plants

Currently, S-CO_2 Brayton cycles have emerged as a promising solution to achieve high efficiency, as well as increased flexibility, in a variety of applications operating with different temperature levels of the heat source, such as fossil-thermal, nuclear, and solar-thermal applications [1–5]. Recent reviews highlight the potential of such cycles: "*S-CO_2 power cycles have several benefits such as high cycle efficiency, small equipment size and plant footprint (and therefore lower capital cost) and the potential for full carbon capture*" [6]; in addition, "*its application includes not only the next generation nuclear reactors but also conventional water-cooled reactors, coal power plants, and several renewable energy sources*" [7]. This latter study points out the need for optimizing the design of these cycles: "*As S-CO_2 cycle performance can vary depending on the layout configuration, further studies on the layouts are required to design a better performing cycle*". In that regard, a number of projects are under development in order to explore both fundamental aspects and technical limitations of crucial unit operations, such as the turbomachinery and heat exchanger [8]. Others are devoted to searching for the optimal process parameter values (i.e., the values of continuous real variables among temperatures, flow rates, pressures, etc.) and maximizing the cycle efficiency for a fixed cycle layout [1,9,10]. Nevertheless, although the cycle layout is an avenue for significant improvement in S-CO_2 Brayton cycles, few studies look at the problem from this perspective.

The present paper aims to apply a process-synthesis approach to the design of a closed Brayton cycle using S-CO_2 as the working fluid. The heat source is a coal furnace, as coal remains the most widespread and cheapest fossil fuel. The general methodology presented here for designing closed power cycles includes the construction of a superstructure containing all relevant possible cycle layouts, the formulation of the cycle synthesis problem as a mathematical optimization problem, and its solution using an appropriate algorithm. Although the start-up of a power plant is important, only steady-state processes were considered in this study.

1.2. Superstructure-Based Design of Power Cycles through the Use of a Commercial Process-Simulation Software

In their seminal article, Umeda et al. introduced the concept of the superstructure and the synthesis problem as follows: "*All the alternative systems are combined into an integrated system and split ratios are introduced at source points where a stream is split into more than two streams. The synthesis problem is solved by determining optimal split ratios at the source points as well as optimal design parameters involved in subsystems*" [11]. In their recent review article about superstructure-based optimization, Mencarelli et al. identified three main sequential steps: "*(i) the postulation of a superstructure, which encapsulates the set of all feasible alternative process structures; (ii) the translation of the superstructure into a mathematical programming model; and (iii) the computation of an optimal structure by solving the mathematical optimization model*" [12].

It is worth noting that the postulation of a superstructure is a central and decisive step that cannot be completely automatized. According to Quaglia et al. [13], the development of the superstructure integrates an alternative collection approach, theinsight-based synthesis approach, and the combinatorial synthesis approach. The first two methods consist in enumerating the known configurations based on previous experiences and using engineering insights to propose new solutions and exclude infeasible or non-conventional alternatives. The combination of different alternatives in a superstructure enables us to enlarge the search space of an alternative flowsheet and thus is likely to include innovative design

solutions. Although not so frequent, the application of superstructure synthesis concepts to the design of power cycles is not new. For an overview of superstructure-based and superstructure-free approaches to designing thermal power plants, the reader is referred to the study by Wang et al. [14]. Various authors have used superstructure optimization for the design of coal-fired plants [15,16], of concentrated solar power (CSP) plants [17,18], of integrated gasification-combined cycle (IGCC) [19], of combined cycles [20,21], of cogeneration or trigeneration systems [22–24], or power cycles for waste-heat recovery [25,26]. The superstructure-based optimization problem involves both discrete and continuous variables and thus can be written as a mixed-integer nonlinear programming (MINLP) problem aimed at minimizing a nonlinear objective function subject to nonlinear constraints [27–29]. Note that generalized disjunctive programming (GDP) can be used as an alternative method to formulate process synthesis problems [29]. Such problems are most often nonconvex (nonconvexity is essentially caused by mass balances and thermodynamics) and exhibit multiple local solutions [30,31]. Solving these complex problems includes the search for optimal values of design (discrete) parameters (defining the process layout) and operational (continuous) parameters (pressure levels, flow rates, etc.) as well as the simulation of the process (i.e., the calculation of the inlets and outlets of all operation units for a fixed layout and given operational parameters). In practice, two different strategies can be considered:

- An *equation-oriented approach* can be selected. This means that the optimization and simulation subproblems are solved simultaneously. This technique is widely used in optimization-based process synthesis, as it offers great robustness for the resolution of highly interconnected systems. However, its resolution necessitates efficient procedures for the initial estimation of process parameters that can be difficult to generate, especially in the case of novel processes for which it is not possible to take benefit from experts' experience [13,32,33]. To simplify the resolution procedure, linear approximation or surrogate models are frequently used to the detriment of solution accuracy [34].
- Otherwise, a *sequential approach* can be used. In this case, the global optimization/simulation problem is split into subproblems that can be solved sequentially. Although this solution path favors the emergence of undesirable local solutions, the gain in simplicity and tractability is important. It enables splitting (at least partially) the optimization and simulation subproblems and, in particular, using well-oiled commercial process-simulation environments for simulating processes. From a historical viewpoint, Harsh et al. [35] interfaced for the first time an outer approximation MINLP procedure with the Flowtran simulator in 1989. Later on, Aspen Plus and Aspen Hysys simulation tools were used in a variety of process synthesis studies such as the design of a distillation processes [36–39] or the retrofit of chemical processes [40–43]. Meanwhile, Wang et al. [16] used a process-simulation software, called Ebsilon Professional, dedicated to the optimization of energy-conversion processes. More recently, Corbetta et al. [44] interfaced the process simulator Avena PRO/II with the GAMS software (MINLP solver) in order to optimize both process layout and parameters. In all the studies mentioned above, the calculation procedure uses an MINLP resolution tool as the master layer calling the process simulator each time a process simulation is needed. As a major drawback, this practice requires major computational efforts. Note additionally that the communication between the process simulator and MINLP algorithms induces additional interfaces and thus additional development efforts. Because such interfaces are not universal, reproducing any of the above-cited studies would require the construction of personalized supporting tools.

In this paper, a simulator-based approach was used to search for the optimal design of a S-CO_2 Brayton cycle. Beyond the case study itself, the scope of this study is primarily methodological: using a superstructure-based optimization technique, it is desired to show how the powerful concepts of this type of process-synthesis approach can be applied to the design of closed power cycles that are more efficient than current ones, from both energetic and economic points of view. Moreover, to the best of the authors' knowledge, it is shown for the first time how to run the superstructure-based optimization loop directly from the

process simulator software, thus avoiding the use of tailor-made interfaces between the MINLP solver and the simulation software. While today, superstructure-based approaches are essentially reserved for experts, the proposed coupling between the solver and the simulation software opens the way to a larger use of this design approach, making it accessible to nonspecialists. The ProSimPlus software was selected here and coupled to an external MINLP solver called MIDACO (for *Mixed-Integer Distributed Ant Colony Optimization*), which is an extension of the ACO (Ant Colony Optimization) metaheuristic algorithm. In addition, this paper differs from most of other superstructure-based optimization studies because of the particularly high number of alternatives considered (more than 1000).

2. Problem Description and Methods

This section describes the formulation of the optimization problem, the specific approach considered to ensure stable and efficient computation of the power cycle model and the proper convergence of solutions.

2.1. Problem Description

Designing a Brayton power cycle involving heat exchangers, turbines, compressors, mixers, and stream splitters as elementary operation units is desired. Because the hot source is a coal-fired boiler, the maximum temperature of the cycle is set to 893.15 K (i.e., 620 °C). The lowest temperature of the cycle is set to 320 K (i.e., 46.9 °C), close to ambient conditions and slightly above the critical CO_2 temperature (which is around 304 K). The CO_2 flow rate in the cooler is set to 6000 kg/s (according to Le Moullec [45], this order of magnitude for the CO_2 flow rate makes it possible to produce around 1 GW of net electrical power). While the choice to specify the CO_2 flow rate rather than the heat duty supplied by the boiler ($\dot{Q}_{Boiler}$) could appear unusual, it can be argued first that this choice has no impact on the final design of the cycle: specifying the CO_2 flow rate and calculating the heat duty ($\dot{Q}_{Boiler}$) in return or doing the opposite is equivalent. Indeed, once the Brayton cycle's architecture and the corresponding electrical power are determined for a fixed flow rate of CO_2 in the cooler, scaling laws enable the calculation of the CO_2 flow rate associated with any specification of the net electrical power. Secondly, from a numerical point of view, the value of the CO_2 flow rate is very sensitive to the cycle architecture for a given heat duty ($\dot{Q}_{Boiler}$), and thus, specifying this heat duty ($\dot{Q}_{Boiler}$) and searching for the corresponding flow rate may induce problems of convergence, explaining why it has been decided to specify the CO_2 flow rate in the cooler. In addition, the cooler flow rate was considered instead of the heater flow rate simply because the cooler is always unique in the Brayton cycles involved in this study, while heating can be split into several devices (including heating from the boiler and the reheating and thermal recuperation of flue-gas thermal energy).

2.2. Software Environment Selection

In a recent paper, Mecheri and Le Moullec highlighted the potential interest of S-CO_2-based Brayton cycles for coal-fired power plants and proposed a design usable for a first step of the implementation of the technology based on realistic industrial modeling hypotheses [9]. The present article takes up most of the hypotheses used by Mecheri and Le Moullec in terms of temperature levels, flow rates, efficiencies of rotating machines etc.

From a technical viewpoint, we decided to use the ProSimPlus™ commercial modular sequential simulator not only for the robustness of the simulation tools it offers but also for the possibility of interfacing the software with external optimization codes or defining tailored unit operations. Such features appeared of special interest for implementing a superstructure-based process design. In particular, they made it possible to include tools for MINLP optimization and for defining connectivity units of superstructures as described in the next section.

In terms of thermodynamic modeling of S-CO_2, it is worth recalling that the simulation, sizing, and optimization of a Brayton cycle are influenced by the selection of an equation of state (EoS) [46]. It has been shown previously that only a multiparameter EoS

designed specifically for the modeling of pure CO_2 properties offers sufficient accuracy in the estimation of phase, energetic and derived properties, particularly in the critical region [46]. According to this study, the Span-Wagner model was selected here.

2.3. Modeling of Flow Switches in the Simulator Environment

In order to define a superstructure within the selected process simulator, i.e., a superior process flowsheet integrating as many promising process layouts as possible [22], it was necessary to define a specific operation unit called a *flow switch*, allowing one to switch from one stream to another and thus giving the possibility to include some equipment in the process and to exclude some others. Therefore, a flow switch makes it possible to virtually remove unit operations by simply annihilating the flow rates of matter passing through. It is similar to a flow splitter, but instead of having a continuous separation ratio, it enables the selection of a preferential path. Note that two types of flow switches were defined: the dual-path switch for selecting one preferential path out of two and the triple-path switch for selecting one path out of three. Figure 1 illustrates the operation of a dual switch with one inlet stream (S_3) and two outlet streams (S_1 and S_2).

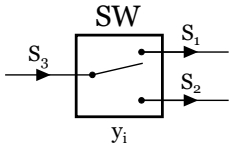

Figure 1. Illustration of a dual-path decision switch. S_k denotes the molar or mass flow rate of stream k and y_i, an integer decision variable used for the selection of the preferential path (see Equation (1)).

Equation (1), involving y_i, an integer decision variable, describes the decision dual-path switch model implemented.

$$\begin{cases} S_1 = S_3, \text{ if } y_i = 1 \\ S_2 = S_3, \text{ if } y_i = 2 \end{cases} \quad (1)$$

Note that in process simulators, a mass flow rate cannot be zero at the entrance of a unit operation. As a consequence, a "zero flow rate" was modeled as a stream with a molar flowrate equal to 10^{-15} mol/s.

2.4. Mathematical Formulation of the Superstructure-Based Design Problem and Resolution Method

2.4.1. Definition of the Main Objective to be Reached

Since the S-CO_2 Brayton cycle is aimed at producing power from thermal energy, the cycle efficiency is an obvious indicator of its performances. It is classically expressed as

$$\eta_{net,cycle} = \dot{W}_{net\ cycle} / \dot{Q}_{hot} \quad (2)$$

where $\dot{W}_{net,cycle}$ is the net power cycle generated from the coupled system {turbine + compressor} and defined by

$$\dot{W}_{net,cycle} = \sum \dot{W}_{turbine} - \sum \dot{W}_{compressor} \quad (3)$$

Note that all power quantities above are positively defined. The heat duty $\dot{Q}_{hot}$ is the heating and reheating thermal powers provided by the heat source (they are also positively defined). As a first attempt, the optimal design was searched naively as the layout maximizing the cycle efficiency. This objective function is deemed as "naive" because the main obvious objective is not coupled to other objectives, which consist of minimizing process costs or energy dissipation. By anticipating our next results, it will be shown in a subsequent part why and how this naive objective function could (or should) be completed.

Eventually, the superstructure optimization problem was expressed as

$$\begin{array}{ll} \underset{x,y}{\text{Min}} & \phi(x,y) = -\eta_{cycle} \quad (x \in \mathbb{R}^{n_{con}}, y \in \mathbb{Z}^{n_{int}}) \\ s.t. & g(x) \geq 0 \\ & x_{min} \leq x \leq x_{max} \\ & y_{min} \leq y \leq y_{max} \end{array} \tag{4}$$

where $g(x)$ is the vector of inequality constraints; x denotes the vector of n_{con} continuous real variables while y is the vector of n_{int} flow switch decision variables; and x and y are both unknown-variable sets that are solutions to the minimization problem defined by Equation (4). As mentioned previously, this latter belongs to the *Mixed-integer nonlinear programming* (MINLP) class of problems.

2.4.2. Selection of an Algorithm for Solving the MINLP Problem

MINLP problems associated with superstructure-based process-design approaches are known to be tricky due to the high degree of non-convexity of most of the functions involved in the problem definition. As mentioned previously, this feature results essentially from models used for describing operation units and thermodynamics. Therefore, the choice of an efficient MINLP solver plays an important role in the success of the whole approach.

On one hand, deterministic MINLP algorithms could be used. They are usually obtained by combining Linear Programming algorithms, Integer Programming, and Nonlinear Programming such as the branch and bound [47], outer approximation [48], and Generalized Benders Decomposition (GBD) [49] methods. Some state-of-the-art deterministic solvers (e.g., alphaBB [50], BARON [51], BONMIN [52], MISQP [53], and COUENNE [54]) were integrated into various high-level algebraic modeling environments (e.g., GAMS and AMPL), tailored for complex, large-scale applications [55]. The above solvers can essentially achieve global optimal solutions for convex problems, but some of them can also be used for non-convex problems.

On the other hand, some stochastic algorithms were specifically derived to solve MINLP problems without requiring explicit expressions of the mathematical models used to estimate the objective function and the related constraints. This feature is of special interest when the process is simulated using a modular simulator software [56]. In particular, stochastic algorithms include nature-inspired algorithms such as the Genetic Algorithms [57–59], Particle Swarm Optimization [60], Tabu search [61], or Ant Colony Optimization (ACO) algorithms [62]. A further advantage of stochastic approaches with respect to deterministic ones lies in their robustness and ability to manage non-convexity or discontinuous function behaviors.

In this study, we decided to take advantage of the flexibility of stochastic solvers through the use of MIDACO (*Mixed-Integer Distributed Ant Colony Optimization*), an extended evolutionary Ant-Colony Optimization algorithm combined with the so-called *Oracle Penalty Function*, which is an approach for constraint handling. More precisely, the central idea of the Ant-Colony Optimization (ACO) algorithm proposed by Dorigo [62] is to mimic the biological behavior of ants randomly searching for food and marking their way back to the anthill with a chemical pheromone when a food source has been found. Over time, the shortest path appears to be the one most traveled by ants and therefore the one with the highest concentration of pheromones. The advanced constraint handling in MIDACO is based on an advanced penalty approach (Oracle penalty function), where a constrained MINLP problem is converted to an unconstrained MINLP problem [63]. This method has shown promising capacity and is already integrated into a number of academic nature-inspired MINLP algorithms [64–66]. Details about the ACO algorithm and constraint handling technique used in MIDACO can be found in the references [63,67].

For most stochastic algorithms, it is generally difficult, if not impossible, to establish a proof of convergence. Nevertheless, Schlüter [68] achieved a comparison between the MIDACO, BONMIN, COUENNE, and MISQP solvers through 100 benchmark problems [69].

His results show that MIDACO is able to find the (already) best-known and sometimes even a better global solution in a reasonable time. Moreover, note that in the review by Bussieck and Vigerske [55], MIDACO is considered a state-of-the-art nature-inspired stochastic solver.

Technically speaking, with the reverse communication available in the commercial solver MIDACO, the optimization block of the simulation software ProSimPlus™ can call this external solver without additional user effort.

To conclude this section, let us mention that the risk of non-convergence and, thus, of failure of the minimization procedure always exists in spite of the inner quality of the simulation software tools and the selected solver. Indeed, the closed nature of a cycle and the presence of recycle streams make the mathematical complexity increase even more, as does the presence of flow switches, which inevitably induce a discontinuous behavior of the objective function. As a consequence, attention has to be paid to convergence issues, and strategies must be implemented to make them easier. These strategies are described in the next section.

2.5. Strategies for Ensuring Convergence

The success of an optimization algorithm is known to be strongly influenced by the problem formulation and the selection of variables, even when using a stochastic optimizer. It is thus important to express the problem in a way that ensures both fast and easy convergence and enables the satisfaction of constraints applying to all process variables [44]. In this study, in order to improve the simulation and optimization convergence, four strategies were implemented and are successively described below.

2.5.1. Selection of a Feasible Path

In a sequential modular simulator (e.g., the ProSimPlus software™), the selection of tear streams is a key lever that facilitates the convergence of flowsheets involving recycle loops. It is recalled that stream variables (temperature, flowrate, pressure) of streams involved in recycle loops cannot be computed in a straightforward way but require iterative calculations (through the tear-stream technique, for instance). A tear stream is a stream whose variables are initially guessed; information is passed then from unit to unit until new values of tear-stream variables are computed. Calculations are repeated until convergence is reached, i.e., until the new values of tear streams are equal to the guessed ones (the corresponding residue equations are named *tear equations*). Note that a tear stream can be any stream (not necessarily a recycle stream) that participates in a recycle loop [33]. In the ProSimPlus™ software, tear variables can be estimated during the simulation step (independently of the optimization step). This method is called *feasible path optimization*.

At this step, it can be mentioned that another option was also possible: to consider tear-stream variables as optimized variables. To do so, each tear stream must be physically split into two inlet and outlet streams, and tear equations must become equality constraints of the optimization problem. This method is named *infeasible path optimization*. In the present case, the first option was preferred to the second one because it helps reduce the number of optimized variables and the computing effort.

While automatic procedures exist to select tear streams [70–73], we decided, however, to specify the same tear stream for simulating all the S-CO_2 Brayton cycles: it was chosen as the cold stream leaving the recuperator HTR and entering into the boiler. As an advantage, the temperature of S-CO_2 at the cooler exit is fixed at 320 K and is not in the optimization variable set. Therefore, selecting this tear stream does not increase the complexity of the optimization problem.

2.5.2. Use of Fictitious Compressors to Control Pressure Ratio in Turbines

In the Brayton cycle superstructures considered in this study, optimal pressure ratios in turbines vary from one layout to another (where optimality is defined by the objective function described in Section 2.4.1). Therefore, these ratios are considered as optimizer

variables subject to constraints: indeed, to guarantee that turbines outlet pressures ($P_{turbine}^{outlet}$) are always higher than the main compressor (C1) inlet pressure (P_{C1}^{inlet}), a constraint inequality must be added: $P_{turbine}^{outlet} > P_{C1}^{inlet}$. However, adding constraints is likely to increase the non-convexity of the optimization problem and thus its complexity. In order to avoid the addition of inequality constraints, a simple solution can be implemented: a fictitious compressor coupled to a fictitious cooler is introduced after each turbine in order to raise the CO_2 turbine outlet pressure to the main compressor inlet pressure in case where the latter would become too low:

$$\begin{array}{ll} \text{if } P_{turbine}^{outlet} < P_{C1}^{inlet} \text{ , then} & P_{turbine+fictitious\ units}^{outlet} = P_{C1}^{inlet} \\ \text{else} & P_{turbine+fictitious\ units}^{outlet} = P_{turbine}^{outlet} \end{array} \quad (5)$$

The cooler is used to fix the temperature of the CO_2 stream exiting from the turbine outlet at the value it would have if the fluid flowed from $P_{turbine}^{inlet}$ to $P_{turbine+fictitious\ units}^{outlet}$ in a single turbine. Then, the required work of the fictitious compressor is added to the electricity consumption term of the cycle efficiency, as detailed in Section 2.4.1. Figure 2 shows a simple superstructure that we used for the validation of the methodology (this validation step is discussed in Section 2.6). This simple superstructure involves such fictitious units and is presented here for illustration.

2.5.3. Management of Recuperator Units

A recuperator is a heat exchanger combining two hot and cold process streams for the thermal integration purpose and thus is an important piece of the optimization strategy. Assuming that inlet streams of the recuperator are fully defined, outlet-stream thermal states were determined here from the knowledge of the specified thermal pinch (defined as the minimal temperature difference between the hot and cold sides of the heat exchanger). Although thermally virtuous, this practice shows a serious drawback for the cycle simulation: the calculation of a cold or hot side outlet state of a given recuperator entails the modification of the inlets and outlets of all subsequent units and, thus, of the hot or cold side inlet of the same recuperator. Consequently, an integrated heat exchanger induces a noticeable increase in the number of iterations required for simulation and is thus prejudicial to the simulation convergence, to the simulation time, and, by extension, to the optimization procedure. To avoid this, we decided to move thermal integration calculations from the simulation block to the optimization block: the recuperator involving two integrated streams was split into two separated streams—a hot-side inlet stream cooled by an external *cold sink* and a cold-side inlet stream warmed by an external *hot source*—as illustrated in Figure 2. These two units were linked in the simulation block by a simple equation constraint that has the advantage of not introducing additional iterations for simulating the cycle (but it does not guarantee an optimal thermal integration of the cycle anymore):

$$-\dot{Q}_{hot\ source} + \dot{Q}_{cold\ sink} = 0 \quad (6)$$

Because optimal thermal integration is obtained when the quantity of power heat transferred from hot to cold sides is maximal, outlet-stream temperatures of heat exchangers were added to the list of optimized variables. In doing so, the optimizer had the possibility to select outlet-stream temperatures to maximize the transferred power heat and thus the cycle efficiency. In order to avoid thermal pinches lower than a specified minimum value, inequality constraints were added to the optimization problem.

Eventually, all these modifications enabled the reduction in the occurrence of diverging iteration processes in the simulation block. The optimization procedure itself benefited from the relaxation induced by the splitting of the counter-current exchanger, although additional parameters (outlier temperatures of recuperators) and inequality constraints (on thermal pinch temperatures) were added.

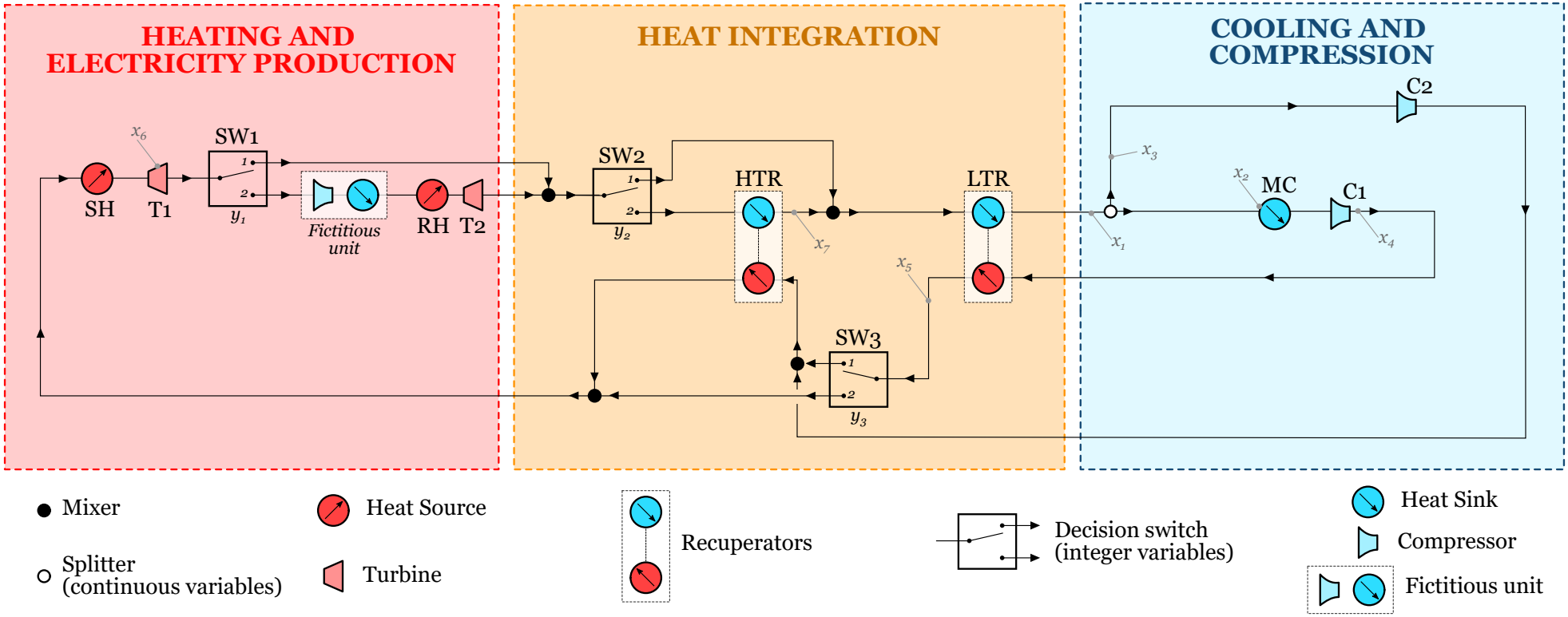

Figure 2. Introduction of fictitious compression + cooler units in the simplified S-CO_2 Brayton cycle superstructure (used for method validation).

2.6. Modeling and Optimization Approach Validation on a Simplified Case

As mentioned previously, a simplified superstructure, introduced in Figure 2, was used to validate the methodology and consequently, included only a few S-CO_2 cycle architectures. Details about this validation procedure are provided in a Supplementary Material File. A more sophisticated superstructure, accounting for near-industrial conditions, is now proposed with the ambition to find out a new cycle architecture that is more efficient than existing structures, with respect to the fixed objectives. In particular, the *preheating* design configuration proposed by Mecheri and Le Moullec [9] for coal-fired power plant applications has been incorporated into this new superstructure. Two types of objectives are considered here: the first one deals with the maximization of energy efficiency, while the second one concerns the minimization of the levelized cost of electricity (LCOE), including operating and design costs.

2.7. Building of a Superstructure Accounting for Realistic Industrial Conditions

In a coal-fired plant, the thermal energy (generated by radiative and convective effects) received by the cycle's working fluid (S-CO_2 here) is provided by the combustion of coal in the boiler. It is assumed that a technology similar to the current state-of-the-art coal boiler, called the *Ultra-Super-Critical (USC) steam boiler*, can be combined with the studied S-CO_2 Brayton cycle. The highest temperature in such a boiler is around 1673.15 K ($\approx$ 1400 °C), corresponding to the flame temperature: approximately half of the total combustion heat duty is produced at this temperature through radiative transfer (this quantity is denoted $\dot{Q}_{boiler}$ and represents the total heat flux used for S-CO_2 main heating and reheating when the latter exists), while the other half is sensible heat (denoted $\dot{Q}_{\text{flue gas}}$), extracted from flue gases leaving the boiler [45], the temperature of which can reach around 823.15 K (550 °C). Even if this sensible heat duty cannot be easily recovered, an integrated network of heat exchangers in the furnace device enables the reuse of a part of the heat duty stemming from flue gases (denoted $\dot{Q}_{\text{recovered from flue gas}}$). In this paper, following orders of magnitude mentioned by Le Moullec and Mecheri [9], it will be assumed that the thermal energy extracted from flue gases that can be reinvested in the process is 9% of the lost thermal energy convected by flue gases.

$$\frac{\dot{Q}_{\text{recovered from flue gas}}}{\dot{Q}_{\text{flue gas}}} = 9\% \tag{7}$$

A graphical summary of the use of the thermal energy produced in the boiler is proposed in the form of a Sankey diagram in Figure 3. Such a thermal integration makes it possible to save a part of the thermal energy required for heating and reheating the working fluid and thus to increase the cycle's efficiency.

Mathematically, Equation (7) will be considered as an equality constraint of the optimization problem. In the superstructure itself, the possibility of preheating S-CO_2 from "free" thermal energy $\dot{Q}_{\text{flue gas}}$ will be included. Without presuming too much about the coming results, it is expected that this possibility will be retained in the final architecture of the cycle.

In addition, the superstructure was built in order to include, as much as possible, most of the S-CO_2 Brayton cycle layouts published in the open literature. To this end, a review conducted by Crespi et al. [74] containing 42 Brayton cycles was considered in addition to the ones mentioned by Le Moullec and Mecheri [9]. The final superstructure proposed here is shown in Figure 4 and enables the reproduction of all the layouts introduced by Le Moullec and Mecheri, as well as 11 out of the 42 cycle architectures described by Crespi et al. The cycle configurations listed in the literature review that were not considered are those relying on transcritical cycles and those utilizing heat sources different from coal combustion, thus leading to atypical cycle configuration (for instance, if a fusion reactor is considered, two main heaters in parallel may be coexisting).

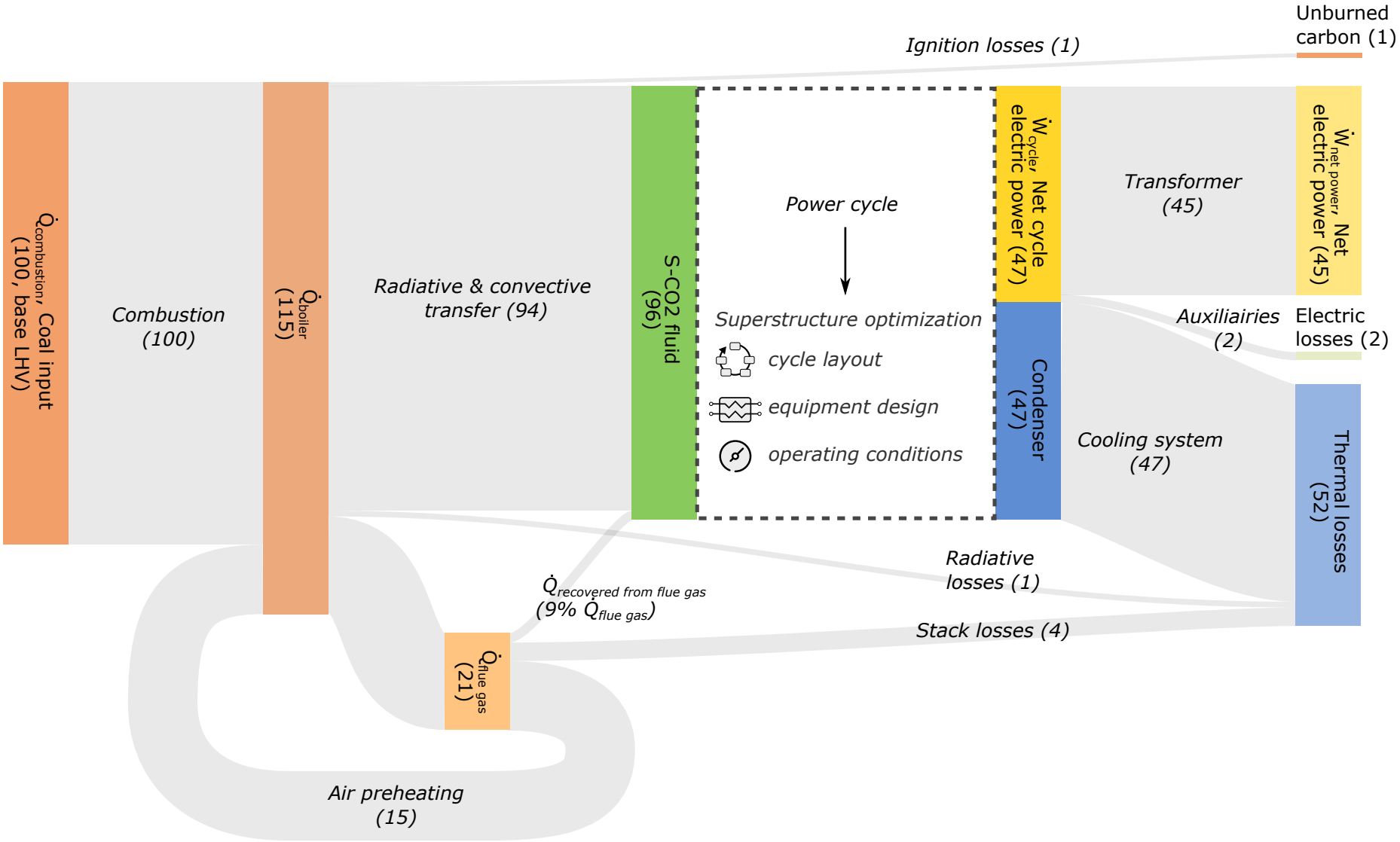

Figure 3. Sankey diagram of the energy (values in parentheses are orders of magnitude that vary according to the net cycle efficiency).

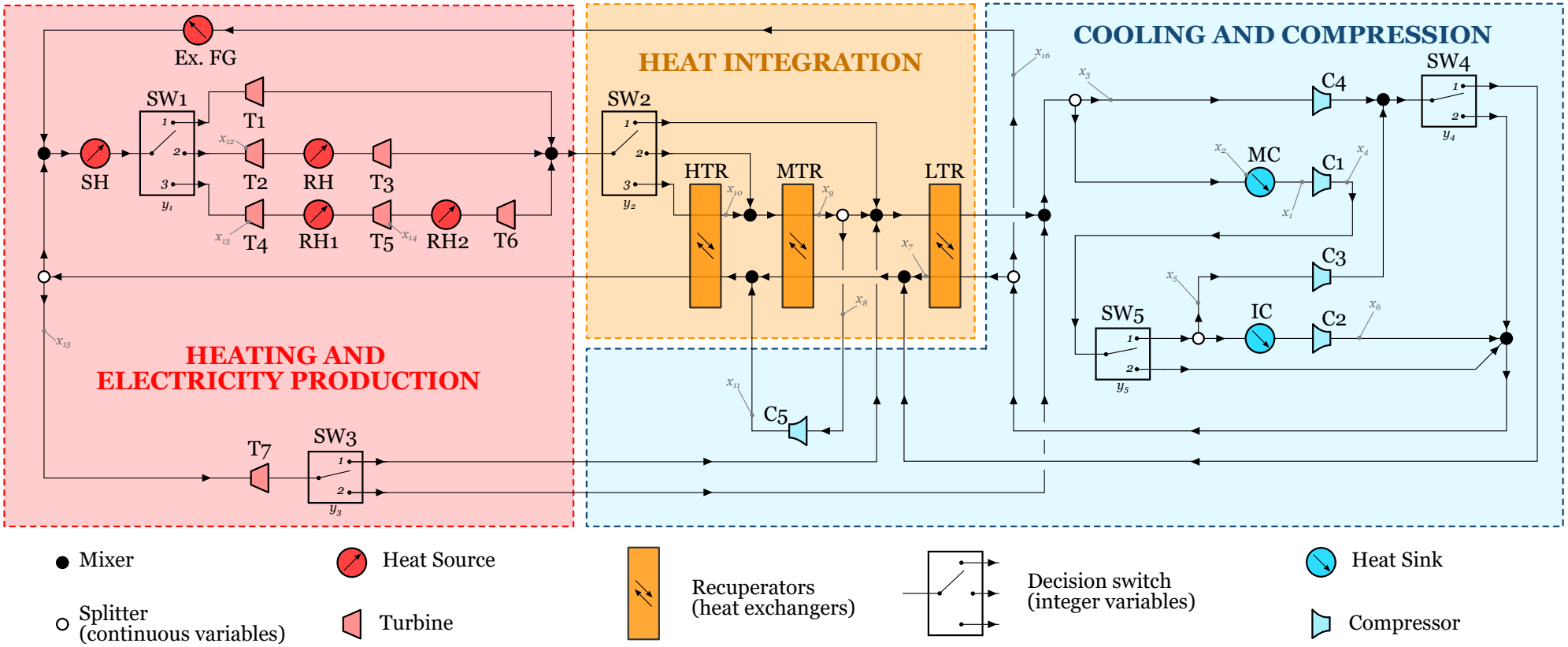

Figure 4. Superstructure used for finding out an optimal layout for a S-CO_2 Brayton cycle. Abbreviations: HTR, MTR, LTR = High-, Medium-, Low-Temperature Recuperator. RH = Reheater. SH = simple heater. Ex FG = heater using flue gases as heat source. SW = Switch unit. MC = main cooler. IC = Intercooling.

Remark about the nomenclature used for identifying the process structures: each cycle contained in the superstructure introduced in Figure 4 can be identified using the following notation:

$$a.RH - b.R - SpExpXXX - c.RC - LTRmix - IC - PrC \quad (8)$$

where

Symbol	Signification (See Figure 4)	Switch Concerned
a., b., and c.	Numerical values (integer)	
a.RH	$a \in \{1;2\}$: number of ReHeat	SW1
b.R	$b \in \{1;2;3\}$: number of recuperators	SW2
SpExpMTR or SpExpLTR	Split expansion = existence of turbine T7 stream. SpExpMTR means $y_3 = 1$; SpExpLTR means $y_3 = 2$	SW3
c.RC	$c \in \{1;2\}$: number of the recompression loop: {c = 1}: existence of C4; {c = 2}: existence of C4 and C5	
LTRmix	C4 outlet is mixed with the inlet of LTR cold side ($y_4 = 2$)	SW4
IC	Existence of Intercooling	SW5
PrC	Existence of pre-compression = existence of C3	

For example: 2RH—3R—1RC—IC stands for the following cycle configuration:

- A double reheated (3 turbines);
- With three recuperators (High-, Medium-, and Low-Temperature recuperators);
- Only one recompression loop (only C4);
- With intercooling;

The superstructure in Figure 4 can be divided into three different blocks: the heat source and electricity-production block, the heat-integration block, and the cooling compression block. From right to left, the first logical flow switch SW1 gives a choice between three options: a single, a double, or no reheating. The second flow switch SW2 in the heat integration block affords the use of recuperators MTR and HTR. Note that recuperator LTR is included in a systematic way in any Brayton cycle of the superstructure. SW3 could also be considered as part of the heat-integration block as it searches for the best location (with respect to the objectives) for injecting the working fluid exiting turbine T7. Similarly to SW3, switch SW4 enables the identification of the best location for reinjecting the flow issued from compressors C3 and C4. Finally, switch SW5 offers the possibility of adding intercooling between compression stages (and thus reducing the operating costs of compression). The proposed superstructure offers no fewer than 540 possible layouts for identifying an optimal version of the S-CO_2 Brayton cycle. This enumeration derives from the possible values of switches (either two-way or three-way) and flow splitters (which can be considered as the continuous versions of the binary switches, including no splitting and partial splitting) variables and by eliminating the combination of variables that lead to identical flowsheet (e.g., values taken by SW3 and SW4 switches have an incidence on the structure only if the flow is positive). As previously mentioned, to simplify the formulation of the optimization problem by avoiding the addition of constraints on the minimum pressure at turbine exits, fictitious {compression + cooling} units were added after turbines T2, T3, and T4 (for the sake of simplicity, they are not represented in Figure 4). In the same idea, a fictitious {expansion + heating} unit was inserted after compressor C2. Eventually, the final superstructure contained 32 unit operations (including the fictitious units).

3. Energy-Optimization-Based Synthesis: Finding a Layout Maximizing the Cycle Efficiency

3.1. Problem Definition

The proposed superstructure is first used for solving a mono-objective optimization problem: the maximization of the cycle efficiency (without consideration of cost constraints). Mathematically, the optimization problem is described by Equation (4), where the cycle efficiency is classically defined as

$$\eta_{Cycle} = \frac{\dot{W}_{\text{net cycle}}}{\dot{Q}_{\text{Boiler}}} \tag{9}$$

where $\dot{Q}_{\text{Boiler}}$ is the power heat supplied by the boiler to S-CO_2 for the main heating, reheating (if it exists), and flue gas recuperator; $\dot{W}_{\text{net cycle}}$ is the net mechanical power obtained by subtracting the electrical power supplied to compressors to the electrical power generated over all the turbo-alternor units. This excludes the power consumption of auxiliary equipment such as coal crushing and transport, induced and forced-draft fan, pump for cooling systems, and depollution equipment, as well as transformer losses.

The 16 continuous variables x_i involved in the optimization problem, as well as the five discrete variables y_i, the list of specified variables, and the list of associated constraints are shown in Table 1.

It can be noticed that outlet pressures of turbines preceding flow switches SW2 or SW3 can be deduced from other pressures present as variables in Table 1 (and, therefore, are not mentioned in this table). For example, the outlet pressure of turbine T4 is equal to either the pressure of the hot stream leaving recuperator HTR or to the one of the stream entering the cold-source cooler (i.e., the pressure of the LTR hot stream outlet).

In the same way, outlet pressures of compressors C3 and C4 are equal to the outlet pressure of C2 and thus do not appear in the list of optimized variables.

Although process costs were apparently not considered in the problem definition, they were implicitly involved through constraints on the thermal pinch afforded in recuperators LTR, MTR, and HTR. This parameter is imposed to be higher than 10 K in order to (i) guarantee the feasibility of the heat transfer between the hot and cold sides and (ii) prevent excessive heat exchange surfaces, which would entail unreasonable CAPEX costs. During the optimization procedure, these thermal pinches are checked only at the entrance or exit of the recuperators (i.e., at the cold or hot ends) but not inside these devices in order to save calculation time and ensure faster convergence. Therefore, two inequality constraints (one for the cold end and one for the hot end) are used for each recuperator. The internal thermal pinch is checked at the end of the optimization procedure to ensure this constraint is respected and that cases that do not hav an internal pinch higher than 10 K are discarded. It can be noted that, due to CO_2's properties, internal pinch issues might take place in an LTR.

Table 1. List of fixed process data, optimization variables, and constraints considered for solving the optimization of the superstructure proposed here, and energy and LCOE optimal solutions found with the ACO algorithm.

Quantity	Range	Values for Energy Optimum	Values for LCOE Optimum
		Type of optimization problem	
		Mono-objective, min of $\{-\eta_{cycle}\}$	Multi-objective, min of $\{-\eta_{cycle}, CAPEX, LCOE\}$
Specifications and equipment data			
T_{it} turbine inlet temperature (K)	Fixed (design assumption)	893.15	893.15
T_{it} turbine inlet temperature after reheating (K)	Fixed (design assumption)	893.15	893.15
CO_2 flowrate before main cooling (kg/s)	Fixed (design assumption)	6000	6000
Minimal pinch ΔT_{min} authorized (K)	Fixed (design assumption)	10	2
Turbine isentropic efficiency (-)	Fixed (design assumption)	0.90	0.90
Compressor isentropic efficiency (-)	Fixed (design assumption)	0.89	0.89
Pressure drop in every unit (% of inlet pressure)	Fixed (design assumption)	1%	1%
Optimization variables (continuous for x_1 to x_{16}, and integer for y_1 to y_5)			
Compressor C1 inlet pressure $P_{C1,in}$ (MPa)	$x_1 \in [3.3; 10]$	7.6	7.5
Cooling S-CO_2 temperature $T_{cooling}$ (K)	$x_2 \in [304.35; 373.15]$	304.35	304.35
Flow to recompression C4 (%)	$x_3 \in [10^{-6}; 0.5]$	0.3	0.22
Compressor C1 outlet pressure $P_{C1,out}$ (MPa)	$x_4 \in [3.3; 30]$	30	30
Flow to recompression C3 (%)	$x_5 \in [10^{-6}; 0.5]$	n.a. ($y_5 = 2$)	n.a. ($y_5 = 2$)
Compressor C2 outlet pressure $P_{C2,out}$ (MPa)	$x_6 \in [3.3; 30]$	n.a. ($y_5 = 2$)	n.a. ($y_5 = 2$)
Recuperator LTR outlet cold temperature (K)	$x_7 \in [304.35; 893.15]$	488.46	483.85
Flow to recompression C5 (%)	$x_8 \in [10^{-6}; 0.5]$	0.08	10^{-6}
Recuperator MTR outlet hot temperature (K)	$x_9 \in [304.35; 893.15]$	498.46	506.18
Recuperator HTR outlet hot temperature (K)	$x_{10} \in [304.35; 893.15]$	n.a. ($y_2 = 2$)	n.a. ($y_2 = 2$)
Compressor C5 outlet pressure $P_{C5,out}$ (MPa)	$x_{11} \in [3.3; 30]$	n.a. ($x_8 = 10^{-6}$)	n.a. ($x_8 = 10^{-6}$)
Turbine T2 pressure ratio (-)	$x_{12} \in [1.0; 5.0]$	n.a. ($y_1 = 3$)	1.61
Turbine T4 pressure ratio (-)	$x_{13} \in [1.0; 5.0]$	1.53	n.a. ($y_1 = 2$)
Turbine T5 pressure ratio (-)	$x_{14} \in [1.0; 5.0]$	1.53	n.a. ($y_1 = 2$)
Flow to turbine T7 (%)	$x_{15} \in [10^{-6}; 0.5]$	10^{-6}	10^{-6}
Flow to preheating by flue gas (%)	$x_{16} \in [10^{-6}; 0.5]$	0.05	0.05
Switch three-way integer variables SW1, SW2	$y_{1,2} \in \{1; 2; 3\}$	3; 2	2; 2
Switch two-way integer variables SW3, SW4, SW5	$y_{3,4,5} \in \{1; 2\}$	n.a.; 1; 2	n.a.; 1; 2

Table 1. *Cont.*

Quantity	Range	Values for Energy Optimum	Values for LCOE Optimum
Constraints (tolerances of 0.5 K for g_1 to g_5, 0.01 for g_6 and 10^{-5} for g_7)			
g_1 on LTR cold-end temperature difference (K)	$(\Delta T - \Delta T_{min}) \geqq 0$	−0.5	4.5
g_2 on LTR hot-end temperature difference (K)	$(\Delta T - \Delta T_{min}) \geqq 0$	−0.5	21.1
g_4 on MTR cold-end temperature difference(K)	$(\Delta T - \Delta T_{min}) \geqq 0$	−0.5	20.2
g_3 on MTR hot-end temperature difference (K)	$(\Delta T - \Delta T_{min}) \geqq 0$	−0.5	46.0
g_5 on HTR hot-end temperature difference (K)	$(\Delta T - \Delta T_{min}) \geqq 0$	n.a.	n.a.
g_6 on ratio of main compressor C1 (-)	$(P_{C1,out}/P_{C1,in} - 1) \geq 0$	53.8	151.2
g_7 on flue gas energy recovered, see Equation (7) (-)	$\frac{\dot{Q}_{\text{recovered from flue gas}}}{\dot{Q}_{\text{flue gas}}} - 0.09 = 0$	-1.4×10^{-6}	-1.3×10^{-6}
Results: objective functions			
Configuration		**2RH-2R-2RC**	**1RH-2R-1RC**
η_{cycle}, cycle net efficiency (%-pts)		**51.37**	**49.35** (2.02%-pts loss)
CAPEX (M$$_{2016}$)		**3338**	**2239** (33% reduction)
LCOE($$_{2016}$/MWh)		**62.5**	**56.5** (10% reduction) (compared to energy optimum)

3.2. Optimal Results (Cycle Efficiency) for Hot/Cold Temperatures of 620 °C/31 °C

In the context of a coal-fired plant built around a state-of-the-art USC-steam boiler, the following modeling assumptions are proposed: the maximum pressure level is set to 30 MPa, and the S-CO_2 temperature exiting from the hot source heat exchanger is set to 893.15 K, i.e., 620 °C.

In order to ensure the robustness of results, four full optimization runs were carried out. The four runs converged towards similar cycle efficiencies and the same cycle structure, as represented in Figure 5. This cycle structure is characterized by the integer vector $\mathbf{y_A} = \{1, 2, 1, 1, 1\}$, which gives the 2RH-2R-2RC configuration: two reheatings of the S-CO_2 in the boiler, two recuperator heat exchangers, and two recompression loops—one around the LTR and one around the MTR. It is associated with a cycle efficiency of 51.37%.

Both of the two recuperators' LTR and MTR pinches reached their minimal thermal pinch (set through constraint equations at 10 ± 0.5 K). There is no HTR involved in this configuration. It can also be highlighted that each recompression loop is set to ensure the minimal thermal pinch is reached at both ends of LTR and MTR, thus minimizing exergy destruction in these heat exchangers.

In addition, as can be noticed from the temperature entropy diagram of Figure 5, both streams three and four are mixed in the isothermal and isobaric conditions, thus leading to isentropic mixing conditions. This result is noticeable as the temperatures and pressures of these input streams were controlled by the optimization routines; therefore, it appears that optimization converged to temperature and pressure conditions associated with reversible processes in both mixers, which is a common rule of thumb for the optimal management of energy and thus for an optimal design. Even when the optimizer needs to balance two antagonist constraints, the optimal solution minimizes the temperature difference between the mixer input streams, such as in point 4 of Figure 5, where the temperature difference is kept around 60 °C. This antagonist constraint comes from, on one hand, the cascade of relationships between the cold-end LTR pinch, the LTR recompression compressor exit temperature, the cold-end MTR inlet temperature, and the MTR recompression compressor exit temperature, which more or less determine the MTR recompression compressor exit temperature, and, on the other hand, by the MTR hot-end exit temperature that is linked to the MTR cold-end pinch.

The pressure ratios in the three turbines are identical and equal 1.53, which is approximately, for an ideal gas expansion–compression sequence using 30 MPa and 7.6 MPa as high and low pressure levels, respectively, the value associated with the maximal net power production (i.e., $(30/7.6)^{(1/3)} \approx 1.6$). Finally, the two continuous process variables $T_{cooling}$ and P_{out} of compressor C1 converged both to the minimal value afforded for this temperature (i.e., 304.35 K) and to the maximum value for the pressure (i.e., 30 MPa). Most of these results were clearly expected and can be interpreted as reliability indicators of the optimization processes.

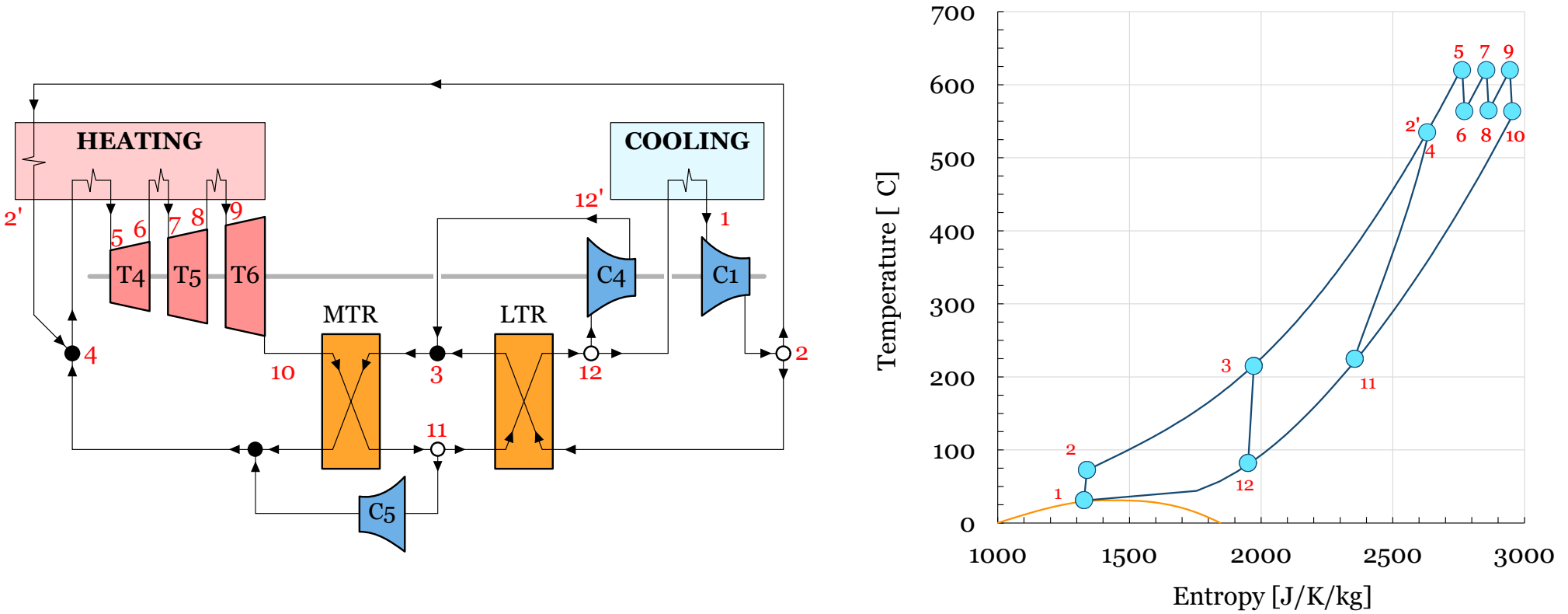

Figure 5. Optimal result obtained from the superstructure optimization. (**left**) Cycle layout (2RH-2R-2RC) and (**right**) corresponding thermodynamic path represented in the temperature–entropy plane.

3.3. Discussion of another High-Performing Cycle Layout

Table 2 lists the 10 configurations leading to higher efficiency and, for each configuration, the corresponding highest efficiency. As a preliminary remark, no precompression or intercooled compression sequence is present among the highest efficiency cycles. Moreover, all these best efficiency configurations show at least one recompression loop that is fully aligned with the conclusion of [9]. Most of these configurations also exhibit two reheats. It is worth noting that only one cycle out of the ten does not include reheat at all. It appears that in the optimal cycle, the first and second reheats allow 1.7%pt and 1.1%pt gain of efficiency, respectively. This is significantly less than for a steam cycle, in which the first reheat operation improves the efficiency by around 5%pt. It can be mentioned that the LTR recompression sequence is systematically present in the 10 best Brayton cycle configurations, thus leading to the conclusion that the LTR is necessary to maximize the cycle efficiency. Note, however, that the addition of a second recompression between the MTR and the HTR induces a gain of efficiency of only ≈0.4%pt.

Table 2. List of the 10 best cycles found via mono-objective maximization of the net cycle efficiency (the corresponding Process Flow Diagrams are shown in the supplementary material file; the structure abbreviation is explained in detail on page 13: for instance, 2RH-2R-2RC stands for a double-reheated—two-recuperators—two-recompression-loops cycle).

Rank	Label	$\eta_{net,\ cycle}$
1	2RH-2R-2RC	51.4%
2	2RH-2R-1RC	50.9%
3	2RH-3R-2RC	50.6%
4	1RH-2R-2RC	50.3%
5	2RH-SpExpMTR-2R-1RC	49.8%
6	2RH-1R-1RC	49.4%
7	2RH-SpExpMTR-1R-2RC	49.0%
8	1RH-1R-2RC	48.9%
9	1RH-SpExpMTR-2R-1RC	48.9%
10	2R-2RC	48.6%

3.4. Effect of S-CO_2 Minimal Temperature on the Cycle Structure and Performance

It is well known that the selection of the minimal cycle temperature has a strong impact on Brayton cycle efficiency, and this remains true for the S-CO_2 cycle. A sensitivity analysis was performed to explore how the choice of the S-CO_2 minimal temperature, within the range [31 °C, 55 °C], influences the cycle configuration and the corresponding main process parameters. For fpir temperatures selected within this range, a full optimization has been carried out. The main results in terms of cycle efficiency are presented in Figure 6.

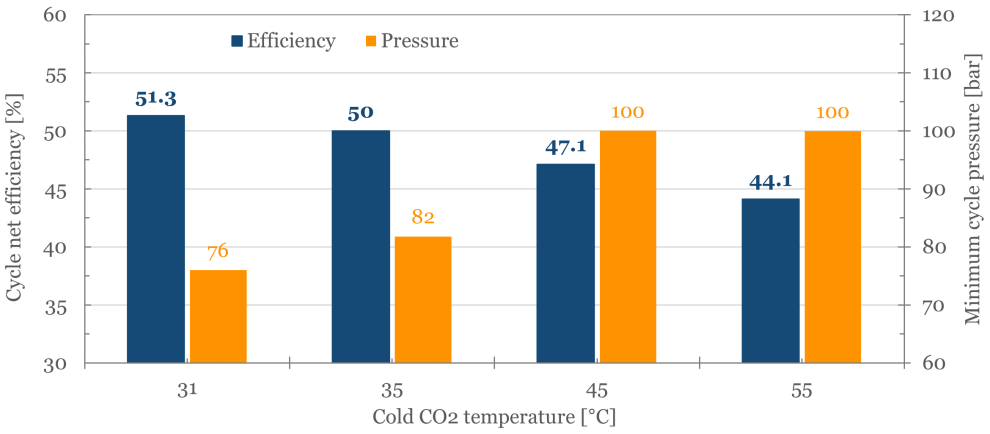

Figure 6. Impact of the CO_2 minimal temperature of the Brayton cycle on (i) the cycle net efficiency and (ii) the minimum cycle pressure. All structures are the same as the base case (2RH-2R-1RC).

Based on these optimization runs, it appears that regardless of the S-CO_2 minimal temperature, the optimal cycle layout remains the same. In all cases, the 2RH-2R-1RC is the best cycle. It is observed that the optimization routine acts on the minimum cycle pressure to mitigate the loss of efficiency induced by warmer cooler conditions. It is also observed that above a cooler temperature of 45 °C, the minimum pressure of the cycle reaches the upper limit of the range, i.e., 100 bar. Eventually, despite this mitigation effect, increasing the S-CO_2 minimal temperature by 10 °C results in decreasing the cycle efficiency by roughly 3%pt.

3.5. Effect of S-CO_2 Maximal Temperatures on the Cycle Structure and Performance

Complementing the sensitivity study performed on the minimal cycle temperature, the maximal cycle temperature has been studied in the range of [580 °C, 800 °C]. It is assumed heremthat such temperatures can be reached by using a boiler similar to the Ultra Super-Critical steam boiler previously described, whose material can withstand 1400 °C (corresponding to the flame temperature). Practically, for four maximal cycle temperatures selected within this range, full optimizations were carried out. The results in terms of cycle efficiency are presented in Figure 7.

It appears that, above 700 °C, the optimal configuration changes from 2RH-2R-1RC to 2RH-3R-1RC. The additional recuperator reduces the overall temperature difference between the S-CO_2 stream exiting the turbine and the S-CO_2 stream entering the boiler. Indeed, with a 10 K pinch constraint, the pinch of the MTR is located on its cold side; therefore, increasing the maximal cycle temperature (when the maximal pressure is kept constant) leads to an increase in this temperature difference.

Finally, it seems that increasing the S-CO_2 maximal cycle temperature by 100 °C results in increasing the cycle efficiency by roughly 3%pt.

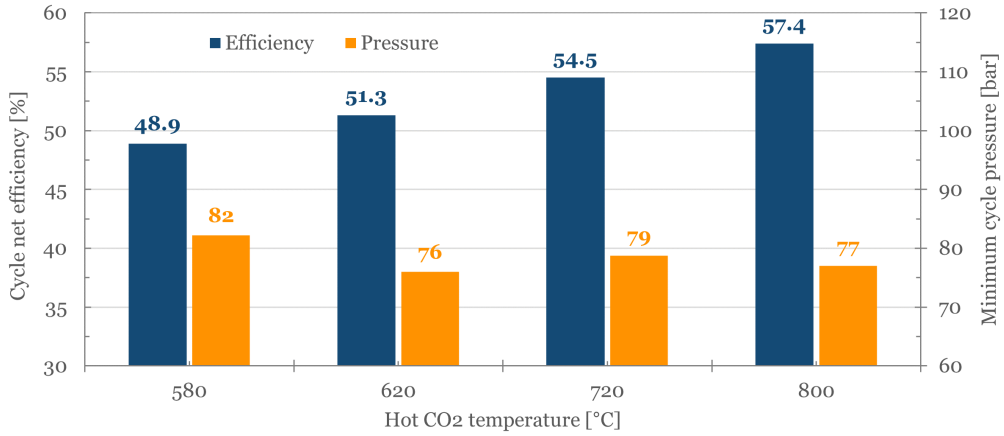

Figure 7. Impact of the CO_2 maximal cycle temperature on (i) the net cycle efficiency and (ii) the minimum cycle pressure. Structures shift from one of the base cases (2RH-2R-1RC) for 580 and 620 °C towards a structure involving an additional recuperator (2RH-3R-1RC) for 720 and 800 °C.

3.6. Sensitivity Analysis of the Pinch Hypothesis

Recuperator pinch values have a significant influence on the cycle efficiency. This section describes a sensitivity analysis regarding the pinches in the LTR and MTR that was performed for the optimal configuration described in the previous section.

For this sensitivity study, all parameters were kept the same as the base case, and only LTR pinch, MTR pinch, or both were changed in the range [2 K to 18 K]. The results are shown in Figure 8. The lower limit of the temperature range (2 K) may seem very low. However, as Kumar et al. recently demonstrated [75], pinches of 2 K are today achievable in the cryogenic gas industry. The properties of S-CO_2 are not very different from those of cryogenic gases, which explains why printed circuit heat exchangers are already being

developed for this gas. Today, both CFD and experimental designs approach 5 K [76,77], which gives us hope of reaching 2 K soon.

The break in slope around 10 K is due to the shift in pinch position from the cold side of the heat exchangers to the hot side, with all other variables held constant. It can be highlighted that reducing the pinch of either the LTR or MTR while keeping the other constant results in virtually no improvement in cycle efficiency. In order to improve the cycle efficiency, both pinches need to be reduced simultaneously. This is an interesting result, because it is more expensive to reduce the MTR pinch due to the quality of the material used to build this heat exchanger, and the design often tends to reduce the pinch only on the heat exchanger built from less expensive material, inn our case, the LTR.

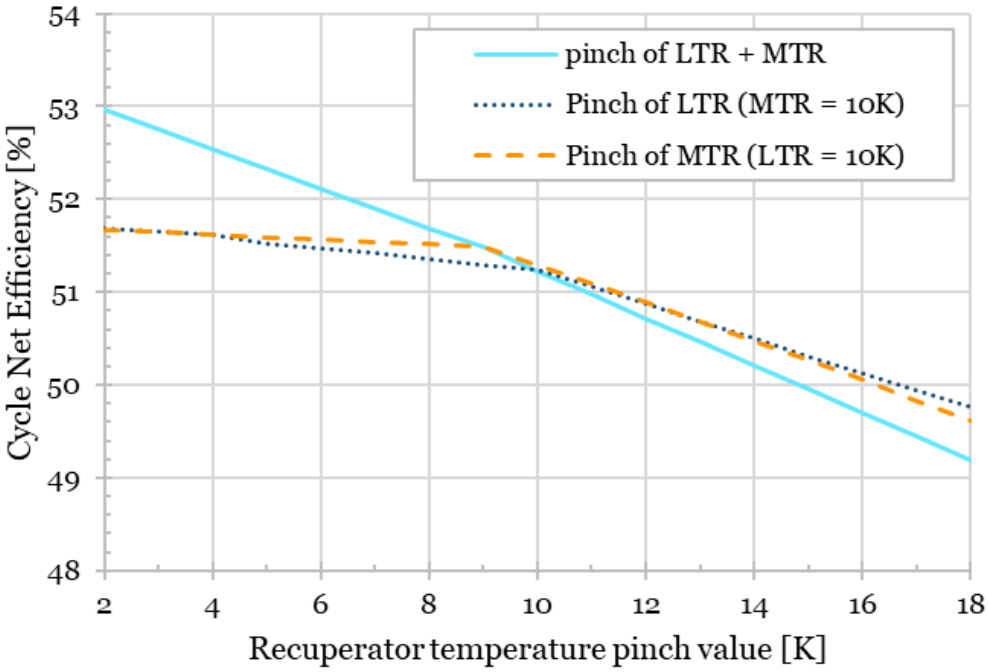

Figure 8. Sensitivity analysis of the pinch values in the recuperators on the cycle efficiency at a fixed structure (2RH-2R-1RC). Three cases were considered here: among the optimal cycle parameters associated with this structure, (i) only the LTR pinch value was modified (dotted line), (ii) only the pinch value of the MTR was modified (dashed line), or (iii), both the LTR and MTR pinch values were modified (continuous line).

Finally, these sensitivity analyses provide insight to help design the optimal S-CO_2 cycle, but the complex interaction between technical constraints (economic obviously, but also those related to the availability of materials) and the cycle configuration require an optimization tool that integrates most of the rules necessary to provide a technically optimal solution. In this respect, a techno-economic approach seems necessary.

4. Multi-Objective Optimization Problem Based on a Techno-Economic Cycle Analysis

4.1. Problem Definition

Optimization based on techno-economic assessment often focuses on the implementation of an exergo-economic analysis [78,79] or on optimizing a key economic function such as the levelized cost of products, the net present value, or the internal rate of return. This approach allows for a single-objective optimization that is very suitable in most cases. Nevertheless, in this work, the economic optimization-based synthesis will be mainly used to help design teams find the best trade-off between different aspects that cannot be summarized in a single economic variable. A multi-objective optimization approach has been preferred, including

- The net cycle efficiency, which reflects the plant's fuel consumption and is therefore directly related to the main operating cost,
- The CAPEX, the overnight capital cost of the plant providing 1000 MW. This parameter could be an interesting way to limit the investment cost for a demonstration project and to assess the interest of the plant operating at a lower load than the base load, and,
- the LCOE, the levelized cost of electricity for base-load power generation, which is the main reason for techno-economic optimization of power plants.

The Pareto front, that is obtained with these three objectives, is interesting to explore designs whose LCOE is close to the one of the optimal design, but with different trade-off between CAPEX and cycle efficiency. Indeed, the layouts showing such LCOE could be studied in detail to find interesting compromises between simplicity, operability and previous industrial experience. This approach seems to the authors to be richer than the definition of a unique objective for the design of a disruption-based innovation process. From this perspective, optimization is the first step of the design process to help the designer focus on a reduced number of relevant configurations.

To improve the readability and usefulness of the results, the economic objectives have been normalized as follows: the reference CAPEX is set at 3340 M$ (from 2020), and the reference LCOE is set at 62 $/MWh. These values correspond to 100 on a normalized scale.

The main difference from energy optimization is that the minimal pinch constraints are reduced to 2 K instead of 10 K; the other variables/bound constraints remain the same (see Table 1 for details on the fixed process data, optimization variables, and constraints).

The methodology for evaluating CAPEX is taken from [80]. It is a bottom-up factorial approach based on the correlation of technical literature. This approach yields low absolute accuracy (often more than 30% deviation) but is useful for comparing different configurations because the correlations used are based on the physical sizing of different pieces of equipment.

The methodology for LCOE evaluation is also taken from [80]. It is a simplified integral approach defined as follows:

$$LCOE = \frac{CAPEX \cdot f_L + OPEX_1}{PROD_1} \tag{10}$$

where $OPEX_1$ and $PROD_1$ are the operating expenses and the electricity produced by the power plant, respectively, during the first year of operation and f_L is the levelization factor, defined as

$$f_L = \frac{l(1+l)^{n-1}}{(1+l)^n - 1} \tag{11}$$

where l is the levelization rate and n is the project duration. Their values are set to 8% and 40 years, respectively. For $OPEX_1$ and $PROD_1$, a base load operation of 7890 operating hours per year is assumed. $OPEX_1$ is calculated as the sum of fuel expenditure (coal at 10 $/MWh$_{th}$ of used coal, base LHV), fixed OPEX (3 % CAPEX per year), and variable OPEX (3.5 $/MWh of electricity produced by the power plant).

4.2. Analysis of the LCOE Optimum

The optimal structure obtained regarding LCOE minimization is represented in Figure 9. This cycle structure is characterized by the integer vector $\mathbf{y_A} = \{1, 1, 1, 1, 1\}$, which produces the 1RH-2R-1RC configuration: one reheating of the S-CO_2 in the boiler, two recuperative heat exchangers, and one recompression loop around the LTR. It is associated with a cycle efficiency of 49.35%.

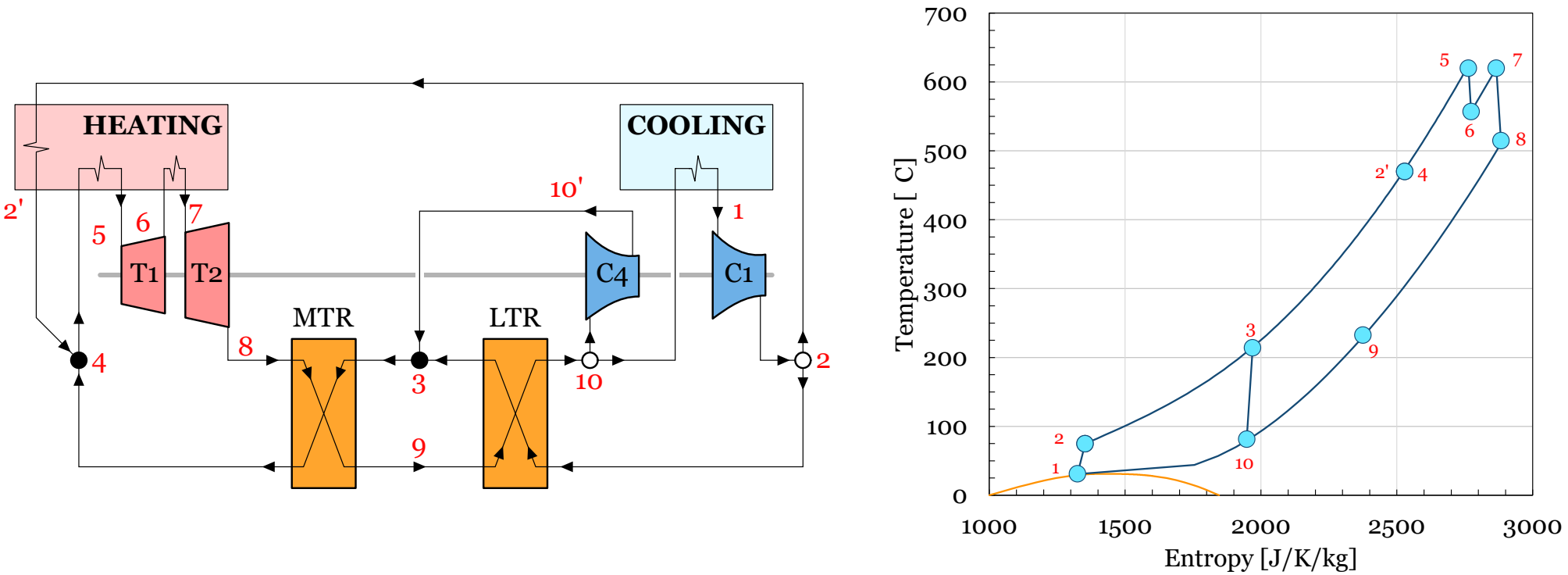

Figure 9. LCOE optimal result obtained from the superstructure optimization. (left) Cycle layout (1RH-2R-1RC) and (right) corresponding thermodynamic path represented in the temperature–entropy plane.

In the optimum-energy cases, the two continuous process variables $T_{cooling}$ and P_{out} of the C1 compressor converged both to the minimal value afforded for this temperature (i.e., 304.35 K) and to the maximum value for the pressure (i.e., 30 MPa).

Besides the deletion of a reheating step in the boiler and the MTR recompression loop, the main differences are the fraction of the flow sent to the LTR recompression loop, which is reduced from 0.30 to 0.22, and the modification of the two heat recuperator pinches: 4.9 K and 22.3 K for the cold- and hot-end temperatures of the LTR, respectively, and 21.6 K and 47.4 K for the cold- and hot-end temperatures of the MTR, respectively.

Regarding economic optimization, there is a clear preference for reducing pinches in the LTR, especially on the cold-end side, most likely for two reasons: the main one is that the thermal energy of the cold-end stream leaving the LTR is rejected in the cold source and therefore lost by the system. This is not the case for other heat exchangers, for which a large pinch results in entropy production but no energy loss. The second reason lies in the material cost of the high-temperature heat exchanger, which drives the trade-off to larger pinches.

Regarding the methodology, while energy optimization parameters are often at the boundary of the range of investigation, this is not the case for economic optimization. This is especially true for heat exchanger pinches. This fact greatly simplifies the convergence of the optimization because the explored solutions are less likely to be found at the boundary of the parameter and constraint spaces, thus reducing the computation burden. On average, 10 times fewer iterations are needed to find the optimum for economic optimization.

4.3. Techno-Economic Pareto-Front

Figure 10 illustrates all the process configurations that have been optimized through the ACO runs. The upper panel illustrates the compromise between the net efficiency and CAPEX, whereas the lower panel illustrates the compromise between the net efficiency and LCOE. Among the 540 configurations that the superstructure is able to represent, those belonging to the Pareto front are mainly the 1RH-2R-1RC configuration, which also has the lowest LCOE.

One might be surprised that the CAPEX could not be reduced more significantly for the low net efficiency power cycle, as one intuitively expects the capital cost to be lower due to low efficiency. Actually, the cost of the boiler is a significant fraction of the overall cost of the power plant, and for a low-efficiency power cycle, a larger boiler is required to provide the same power output. The cost of this larger boiler offsets the reduced cost of the low-efficiency power cycle, leading to the trends shown in Figure 10.

Four specific simulations, the results of which are located on the Pareto front, have been selected for further analysis. They are highlighted in Figure 10, and some of their key attributes are listed in Table 3. These four configurations correspond to the cases where (1) the CAPEX is minimum (yellow triangle), (2) the LCOE is minimum (blue dot), (3) the efficiency is maximum (not shown on the figure to avoid enlarging the scale, but the green star corresponds to the same configuration with technical optimization constraints), and (4) a compromise between high efficiency and a low LCOE (light orange square).

Among these four cases, the only one whose configuration is not 1RH-2R-1RC is the third one, which is characterized by maximum efficiency. In line with our previous results (see Table 2), the maximum-efficiency case corresponds to the 2RH-2R-2RC configuration. The highest efficiency reported in Table 3 is higher than the one reported in Table 2 for the 2RH-2R-2RC configuration because the pinch constraint has been released from 10 K to 2 K, and, as expected, these boundaries were reached through optimization. As already mentioned, all other cases have the configuration 1RH-2R-1RC, and the difference between them is the pinch value in the LTR and MTR recuperators. Indeed, as shown in Table 3, the maximum and minimum pressures and temperatures are the same for all four cases. The simulation results (see Table 3) highlight that the critical pinch to be minimized is clearly the cold end of the LTR, whose value ranges from 6 K to 2 K while the MTR pinch ranges from 29 K to 2 K. This difference can be explained by the low inlet temperature to

the cooler. There is an almost linear relationship between this temperature and the cycle net efficiency. Regarding the CAPEX, the reduction in the pinch value results in a significant increase in recuperator costs and higher cycle efficiency, leading to a smaller boiler, which, however, does not compensate for this increase.

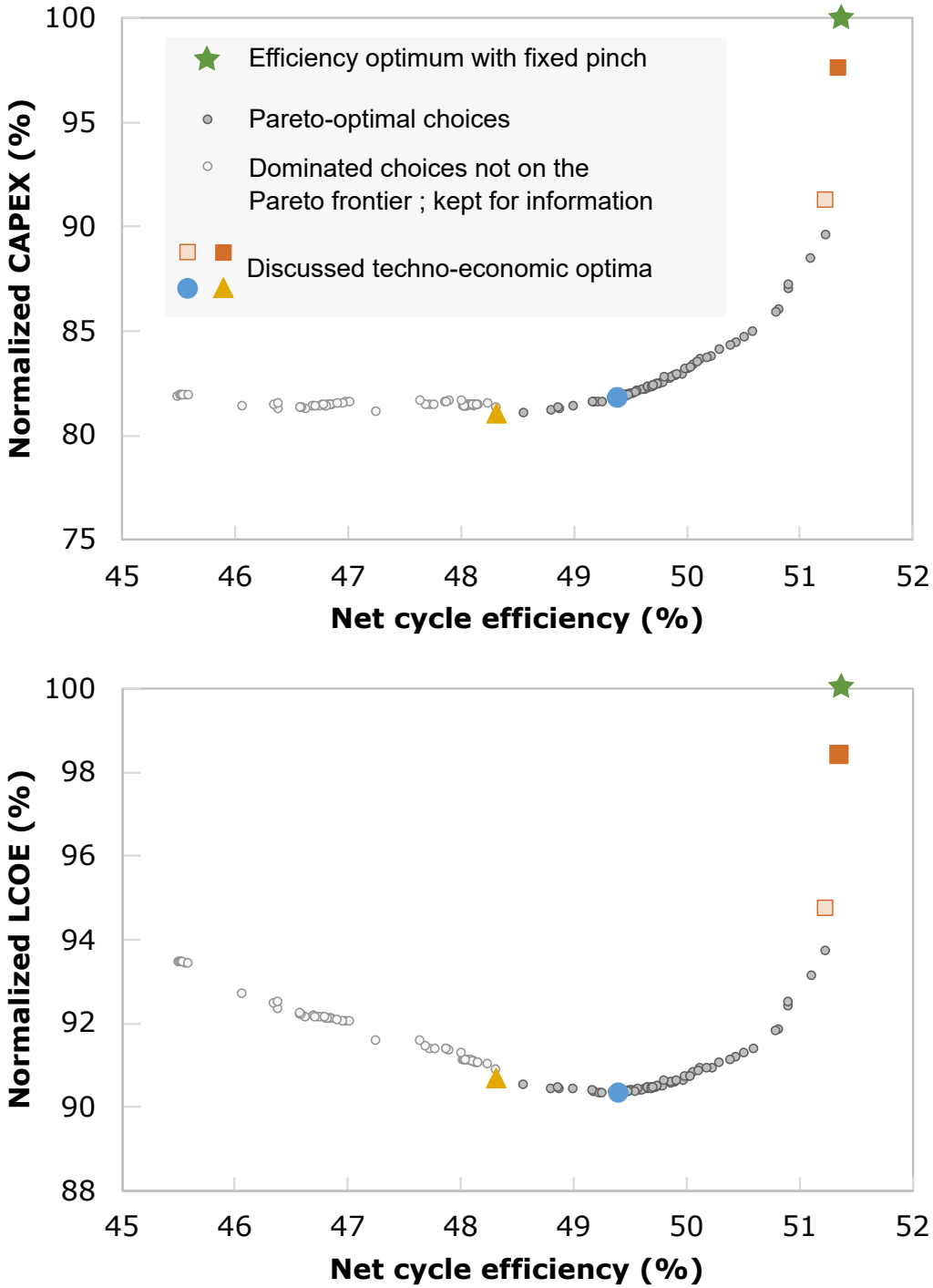

Figure 10. Pareto-front obtained through three-objectives (net cycle efficiency, CAPEX, LCOE) optimization of the superstructure (coloring according to LCOE).

While the lowest CAPEX and the lowest LCOE are very close cases, the case with te highest cycle efficiency entails a very significant increase in CAPEX that leads to a 50% increase in LCOE. This highlights that the CAPEX is a key factor for identifying the optimal configuration in terms of LCOE.

Table 3. Details of the 4 highlighted points on the Pareto Front.

	Unit	Lowest CAPEX	Lowest LCOE	High Eff Compromise	Highest Efficiency
Configuration		**1RH-2R-1RC**	**1RH-2R-1RC**	**1RH-2R-1RC**	**2RH-2R-2RC**
net cycle efficiency	%	48.28	49.35	51.31	52.65
CAPEX	M$	2217	2239	2673	5040
LCOE	$/MWh	56.7	56.5	61.7	93.4
net plant efficiency	%	43.59	44.55	46.3	47.53
Net power	MW	1000	1000	1000	1000
Pmin	bar	75.1	75.2	75.0	75.5
Pmax	bar	298	300	298	300
Tmin	°C	31	31	31	31
Tmax	°C	620	620	620	620
Cooler inlet T	°C	81.4	79.7	77.0	73.8
Boiler inlet T	°C	467	467	497	562
Pinch LTR	K	6.0	4.9	2.8	2
Pinch MTR	K	29.3	21.6	10.5	2
CAPEX fraction					
Compressors	%	1.2	1.3	1.1	0.8
Turbines	%	11.4	11.4	9.7	5.6
Recuperators	%	5.6	7.0	19.0	44.4
Cooler	%	0.9	0.9	0.7	0.4
Boiler	%	54.4	52.9	43.0	22.3
Direct cost	%	19.1	19.1	19.1	19.1
Indirect cost	%	7.4	7.4	7.4	7.4

4.4. Discussion

In all optimized cases for both technical and economical driven problems, the maximum and minimum temperatures and pressures of the cycle are the same:

- The minimum and maximum cycles' temperature values are always found at the boundary of the variable space. This last result can be explained simply by invoking the expression of the Carnot efficiency, which is maximal when the temperature of the cold source is minimal and that of the hot source maximal.
- Regarding the pressures, setting the minimum cycle temperature fixes the minimum optimal pressure of the cycle, and once the first pressure is minimized, so is the second. Therefore, the maximal pressure of the cycle is always set to its highest possible value.

It can be noted that all these results were fully expected.

Regarding energy optimization, the results are also in line with what could be expected: in the case of a more advanced thermal integration of the cycle such as the one with two reheating sequences and two recompression loops, the third recuperator was not selected because, at such a high temperature, the pinch issue is less sensitive and, in addition, already 9% of the overall cold S-CO_2 is bypassed through the flue gas economizer. The results of this optimization are, therefore not surprising and can be considered as a validation of the overall methodology. With the lower constraints of the economical optimization (reduced minimal pinch from 10 to 2 K), the highest efficiency is found for the same configuration (as the optimum energy configuration discussed above) with a more thorough energy integration through pinch minimization. This highlights the key importance of the selection of heuristics for purely technical optimization.

Regarding economical optimization, it is interesting to highlight that a number of specific well-known S-CO_2 Brayton cycle configurations are not present in the Pareto front. Notably, no precompression and no intercooled compression cycles are present. Compared to the previous cases resulting from an energy-based optimization, all configurations with

a double recompression and most configurations with a double reheating sequence were discarded during economic optimization.

The optimal cases in terms of CAPEX and LCOE objectives share the same configuration but exhibit different arrangements of recuperator pinches. Indeed, in the central part of the Pareto front, a unique configuration dominates all the configurations allowed by the superstructure. Since all the best configurations' variations are only based on the design of recuperators, it can be concluded that the optimization results are sensitive to the correlation used for this piece of equipment, and thus, efforts should be made by R&D departments to improve the accuracy of such cost correlations. Note that in the present study, a very specific technology for S-CO_2 cycles was considered, namely printed circuit heat exchangers, which are currently not widely used in industrial applications. Interestingly, this best configuration allows largely higher efficiency than the one achieving the best LCOE. Note that this better performance is simply due to an improvement in heat integration making it possible to decrease operating costs. This trade-off is clearly linked to the expected operating pattern of the plant. In our case, base load operations have been selected, but the economic optimum should be different for semi-base load or peaking load.

This is a strong interest of the analysis of the Pareto front, which enables different configurations that achieve close performance in terms of techno-economical optimization to be stuiedy but could show other features that are not as easy to quantify. For instance, the simplicity of design, the maturity of the industrial use of equipment and material, the maintainability, and the selection of flexible and robust operations are some criteria that can be taken into account to select one configuration over another. The methodology proposed in this article allows the project design team to quickly select the most promising configuration that will be studied in depth as different constraints and opportunities arise.

Finally, it would be very interesting to compare our results with the steam-cycle results obtained by applying the same methodology. This would enable us to compare our results with the current state of the art and with potential improvements in the steam cycle design. To do this, the boiler design must be integrated into the superstructure, and an associated detailed cost model should be developed, probably through a simplified radiative compartmental model coupled with a convective-radiative heat exchanger network that should be integrated into the superstructure. This is clearly outside the scope of the present work and will be a clear follow-up to this article. The inability to compare with a reference steam power plant is the reason why the turbo-machinery efficiency was selected conservatively. If a comparison is to be made, specific work regarding isentropic/polytropic efficiencies and shaft leakage will be required.

5. Conclusions and Perspectives

This work presents a superstructure optimization methodology based on a commercial process simulation software (PROSIM) and a commercial optimizer (MIDACO) and an application case dealing with the optimization of a S-CO_2 cycle for a coal-fired power plant, continuing the work of [9]. This approach is preferred in order to demonstrate that this type of methodology and the corresponding tools can be easily used by engineering teams of R&D departments, thus allowing the devlopment of a tailor-made design for a specific problem.

The work highlights the clear limit of a purely technical optimization approach that does not include an economical layer. Indeed, in such a case, the result of optimization may be nonconclusive because it hides economical constraints in the selection of the technical optimization bounds in the form of minimal pinch constraints, for example.

Regarding the maximization of the mono-objective net cycle efficiency, the energy optimum for our problem is reached by incorporating a double-reheating and double-recompression sequence within the cycle, with two recuperators as well. A net cycle efficiency of 51.4% is then obtained. Moving to the multi-objective techno-economic optimization, with the released constraints (minimal pinch reduced from 10 K to 2 K), the net cycle efficiency can reach 52.7%, but this configuration has a cost of production of electricity 50% higher than the optimal economic solution configuration identified, i.e., the one

with the lowest LCOE. This best economic configuration has only one reheating and one recompression loop and still involves two recuperators for a net cycle efficiency of 49.4% and a cost of electricity of 57 $/MWh, which is 10% lower than the one of the best cycle obtained from an energy-based optimization. This highlights that the present multi-objective optimization, based on a techno-economic approach, leads to more relevant designs than those obtained from engineering heuristics. We here mean that selecting the configuration with the the highest efficiency is not always the best choice, as it often leads to a higher cost of electricity than in the case where the CAPEX is included in the optimization process. The Pareto front analysis highlights that all the cycles emerging from a compromise between CAPEX, LCOE and net cycle efficiency have the same structure, which is the one leading to the optimal cost of electricity. The variants of this configuration along the Pareto front only differ by the thermal pinches in the key heat exchangers, i.e., the recuperators.

However, our results must be considered as partial regarding the potential of the S-CO_2 cycle for coal-fired power plant because, as shown in this work, the coal boiler represents more than 50% of the overall investment cost and the design of the boiler has not been integrated into our superstructure. Adding these two criteria to our optimization is an extension of the proposed work that will be considered in the close future. This will allow the S-CO_2 cycle to be compared correctly with the reference steam cycle.

Regarding the potential evolution of the methodology, the first step should be to test it on another industrial design problem to ensure the robustness of the approach. Accounting for the propagation and treatment of uncertainties throughout the optimization process will enable us to demonstrate the reliability of the results. Finally, as the interest in the techno-economical optimization approach is linked to the extrapolability of its results, a dedicated work to build simple and robust cost functions for equipment and environmental factors should be carried out.

Supplementary Materials: The following supporting information can be downloaded at https://www.mdpi.com/article/10.3390/en16145470/s1. *Validation of the proposed approach using a simplified superstructure*. References [9,81,82] are citation in supplementary materials.

Author Contributions: Conceptualization, M.M., T.N., R.P. and Y.L.M.; Methodology, Y.L.M.; Software, Q.Z., M.M. and T.N.; Validation, M.M., T.N., R.P. and J.-N.J.; Investigation, Q.Z.; Writing—original draft, Q.Z.; Writing—review and editing, M.M., T.N., R.P., J.-N.J. and Y.L.M.; Supervision, R.P. and J.-N.J.; Project administration, J.-N.J. All authors have read and agreed to the published version of the manuscript.

Funding: This research received no external funding.

Data Availability Statement: No new data were created or analyzed in this study. Data sharing is not applicable to this article.

Conflicts of Interest: The authors declare no conflict of interest.

Nomenclature

ACO	Ant Colony Optimization
C_i	Compressor (i = numbering)
Ex. FG	Exhaust Flue Gases
HTR	High Temperature Recuperator
LTR	Low Temperature Recuperator
MC	Main Cooling
MTR	Medium (intermediate) Temperature Recuperator
P	Pressure
RH	ReHeating
SH	SuperHeating
SW	Switch (integer variables)
T	Temperature
T_i	Turbine (i = numbering)

References

1. Dostal, V.; Driscoll, M.J.; Hejzlar, P. A Supercritical Carbon Dioxide Cycle for next Generation Nuclear Reactors. Ph.D. Thesis, MIT, Cambridge, MA, USA, 2004.
2. Kato, Y.; Nitawaki, T.; Muto, Y. Medium temperature carbon dioxide gas turbine reactor. *Nucl. Eng. Des.* **2004**, *230*, 195–207. [CrossRef]
3. Zhang, X.; Yamaguchi, H.; Uneno, D. Experimental study on the performance of solar rankine system using supercritical CO_2. *Renew. Energy* **2007**, *32*, 2617–2628. [CrossRef]
4. Jeong, W.S.; Lee, J.I.; Jeong, Y.H. Potential improvements of supercritical recompression CO_2 brayton cycle by mixing other gases for power conversion system of a SFR. *Nucl. Eng. Des.* **2011**, *241*, 2128–2137. [CrossRef]
5. Neises, T.; Turchi, C. A comparison of supercritical carbon dioxide power cycle configurations with an emphasis on csp applications. *Energy Procedia* **2014**, *49*, 1187–1196. [CrossRef]
6. Zhu, Q. Innovative power generation systems using supercritical CO_2 cycles. *Clean Energy* **2017**, *1*, 68–79. [CrossRef]
7. Ahn, Y.; Bae, S.J.; Kim, M.; Cho, S.K.; Baik, S.; Lee, J.I.; Cha, J.E. Review of supercritical CO_2 power cycle technology and current status of research and development. *Nucl. Eng. Technol.* **2015**, *47*, 647–661. [CrossRef]
8. Ma, Y.; Liu, M.; Yan, J.; Liu, J. Thermodynamic study of main compression intercooling effects on supercritical CO_2 recompression brayton cycle. *Energy* **2017**, *140*, 746–756. [CrossRef]
9. Mecheri, M.; Le Moullec, Y. Supercritical CO_2 Brayton cycles for coal-fired power plants. *Energy* **2015**, *103*, 758–771. [CrossRef]
10. Maio, D.V.D.; Boccitto, A.; Caruso, G. Supercritical carbon dioxide applications for energy conversion systems. *Energy Procedia* **2015**, *82*, 819–824. [CrossRef]
11. Umeda, T.; Hirai, A.; Ichikawa, A. Synthesis of optimal processing system by an integrated approach. *Chem. Eng. Sci.* **1972**, *27*, 795–804. [CrossRef]
12. Mencarelli, L.; Chen, Q.; Pagot, A.; Grossmann, I.E. A review on superstructure optimization approaches in process system engineering. *Comput. Chem. Eng.* **2020**, *136*, 106808.
13. Quaglia, A.; Gargalo, C.L.; Chairakwongsa, S.; Sin, G.; Gani, R. Systematic network synthesis and design: Problem formulation, superstructure generation, data management and solution. *Comput. Chem. Eng.* **2015**, *72*, 68–86. [CrossRef]
14. Wang, L.; Yang, Z.; Sharma, S.; Mian, A.; Lin, T.E.; Tsatsaronis, G.; Maréchal, F.; Yang, Y. A Review of Evaluation, Optimization and Synthesis of Energy Systems: Methodology and Application to Thermal Power Plants. *Energies* **2018**, *12*, 73. [CrossRef]
15. Wang, L.; Yang, Y.; Dong, C.; Morosuk, T.; Tsatsaronis, G. Systematic optimization of the design of steam cycles using MINLP and differential evolution. *J. Energy Resour. Technol.* **2014**, *136*, 031601. [CrossRef]
16. Wang, L.; Yang, Y.; Dong, C.; Morosuk, T.; Tsatsaronis, G. Parametric optimization of supercritical coal-fired power plants by minlp and differential evolution. *Energy Convers. Manag.* **2014**, *85*, 828–838. [CrossRef]
17. Peng, X.; Root, T.W.; Maravelias, C.T. Optimization-based process synthesis under seasonal and daily variability: Application to concentrating solar power. *Aiche J.* **2019**, *65*, e16458. [CrossRef]
18. Ma, Y.; Morosuk, T.; Luo, J.; Liu, M.; Liu, J. Superstructure design and optimization on supercritical carbon dioxide cycle for application in concentrated solar power plant. *Energy Convers. Manag.* **2020**, *206*, 112290. [CrossRef]
19. Jiang, L.; Lin, R.; Jin, H.; Cai, R.; Liu, Z. Study on thermodynamic characteristic and optimization of steam cycle system in igcc. *Energy Convers. Manag.* **2002**, *43*, 1339–1348. [CrossRef]
20. Grekas, D.N.; Frangopoulos, C.A. Automatic synthesis of mathematical models using graph theory for optimisation of thermal energy systems. *Energy Convers. Manag.* **2007**, *48*, 2818–2826. [CrossRef]
21. Ahadi-Oskui, T.; Alperin, H.; Nowak, I.; Cziesla, F.; Tsatsaronis, G. A relaxation-based heuristic for the design of cost-effective energy conversion systems. *Energy* **2006**, *31*, 1346–1357. [CrossRef]
22. Ahadi-Oskui, T.; Vigerske, S.; Nowak, I.; Tsatsaronis, G. Optimizing the design of complex energy conversion systems by branch and cut. *Comput. Chem. Eng.* **2010**, *34*, 1226–1236. [CrossRef]
23. Aviso, K.B.; Tan, R.R. Fuzzy p-graph for optimal synthesis of cogeneration and trigeneration systems. *Energy* **2018**, *154*, 258–268.
24. Voll, P.; Klaffke, C.; Hennen, M.; Bardow, A. Automated superstructure-based synthesis and optimization of distributed energy supply systems. *Energy* **2013**, *50*, 374–388.
25. Kermani, M.; Wallerand, A.S.; Kantor, I.D.; Maréchal, F. Generic superstructure synthesis of organic rankine cycles for waste heat recovery in industrial processes. *Appl. Energy* **2018**, *212*, 1203–1225.
26. Manente, G.; Costa, M. On the Conceptual Design of Novel Supercritical CO_2 Power Cycles for Waste Heat Recovery. *Energies* **2020**, *13*, 370. [CrossRef]
27. Grossmann, I.E. *Minlp Optimization Strategies and Algorithms for Process Synthesis*; Cache-Elsevier: Amsterdam, The Netherlands, 1990.
28. Floudas, C.A. Nonlinear and mixed-integer optimization. fundamentals and applications. *J. Glob. Optim.* **1998**, *12*, 108–110.
29. Trespalacios, F.; Grossmann, I. Review of mixed-integer nonlinear and generalized disjunctive programming methods. *Chem. Ing. Tech.* **2014**, *86*, 991–1012.
30. Quesada, I.; Grossmann, I.E. Global optimization of bilinear process networks with multicomponent flows. *Comput. Chem. Eng.* **1995**, *19*, 1219–1242. [CrossRef]
31. Trespalacios, F.; Grossmann, I.E. Cutting planes for improved global logic-based outer-approximation for the synthesis of process networks. *Comput. Chem. Eng.* **2016**, *90*, 201–221.

32. Dowling, A.W.; Biegler, L.T. A framework for efficient large scale equation-oriented flowsheet optimization. *Comput. Chem. Eng.* **2015**, *72*, 3–20. [CrossRef]
33. Biegler, L.T. *Nonlinear Programming: Concepts, Algorithms, and Applications to Chemical Processes*; Society for Industrial and Applied Mathematics: Philadelphia, PA, USA, 2010.
34. Chen, Q.; Grossmann, I.E. Recent developments and challenges in optimization-based process synthesis. *Annu. Rev. Chem. Biomol. Eng.* **2017**, *8*, 249–283.
35. Harsh, M.G.; Saderne, P.; Biegler, L.T. A mixed integer flowsheet optimization strategy for process retrofits-the debottlenecking problem. *Comput. Chem. Eng.* **1989**, *13*, 947–957. [CrossRef]
36. Bravo-Bravo, C.; Segovia-Hernández, J.G.; Gutiérrez-Antonio, C.; Durán, A.L.; Bonilla-Petriciolet, A.; Briones-Ramírez, A. Extractive dividing wall column: Design and optimization. *Ind. Eng. Chem. Res.* **2010**, *49*, 3672–3688.
37. Leboreiro, J.; Acevedo, J. Processes synthesis and design of distillation sequences using modular simulators: A genetic algorithm framework. *Comput. Chem. Eng.* **2004**, *28*, 1223–1236. [CrossRef]
38. Gutiérrez-Antonio, C.; Briones-Ramírez, A. Pareto front of ideal petlyuk sequences using a multiobjective genetic algorithm with constraints. *Comput. Chem. Eng.* **2009**, *33*, 454–464.
39. Caballero, J.A.; Milan-Yanez, D.; Grossmann, I.E. Rigorous design of distillation columns: Integration of disjunctive programming and process simulators. *Ind. Eng. Chem. Res.* **2005**, *44*, 6760–6775. [CrossRef]
40. Diwekar, U.M.; Grossmann, I.E.; Rubin, E.S. An minlp process synthesizer for a sequential modular simulator. *Ind. Eng. Chem. Res.* **1992**, *31*, 313–322. [CrossRef]
41. Gross, B.; Roosen, P. Total process optimization in chemical engineering with evolutionary algorithms. *Comput. Chem. Eng.* **1998**, *22*, S229–S236. [CrossRef]
42. Brunet, R.; Reyes-Labarta, J.A.; Guillén-Gosálbez, G.; Jiménez, L.; Boer, D. Combined simulation optimization methodology for the design of environmental conscious absorption systems. *Comput. Chem. Eng.* **2012**, *46*, 205–216. [CrossRef]
43. Chen, Y.; Eslick, J.C.; Grossmann, I.E.; Miller, D.C. Simultaneous process optimization and heat integration based on rigorous process simulations. *Comput. Chem. Eng.* **2015**, *81*, 180–199.
44. Corbetta, M.; Grossmann, I.E.; Manenti, F. Process simulator-based optimization of biorefinery downstream processes under the generalized disjunctive programming framework. *Comput. Chem. Eng.* **2016**, *88*, 73–85. [CrossRef]
45. Le Moullec, Y. Conception of a pulverized coal fired power plant with carbon capture around a supercritical carbon dioxide Brayton cycle. *Energy Procedia* **2013**, *37*, 1180–1186. [CrossRef]
46. Zhao, Q.; Mecheri, M.; Neveux, T.; Privat, R.; Jaubert, J.N. Selection of a proper equation of state for the modeling of a supercritical CO_2 brayton cycle: Consequences on the process design. *Ind. Eng. Chem. Res.* **2017**, *56*, 6841–6853. [CrossRef]
47. Gupta, O.K.; Ravindran, A. Branch and bound experiments in convex nonlinear integer programming. *Manag. Sci.* **1985**, *31*, 1533–1546. [CrossRef]
48. Duran, M.A.; Grossmann, I.E. An outer-approximation algorithm for a class of mixed-integer nonlinear programs. *Math. Program.* **1984**, *35*, 307–339.
49. Geoffrion, A.M. Generalized benders decomposition. *J. Optim. Theory Appl.* **1972**, *10*, 237–260. [CrossRef]
50. Adjiman, C.S.; Androulakis, I.P.; Floudas, C.A. Global optimization of mixed-integer nonlinear problems. *Aiche J.* **2000**, *46*, 1769–1797. [CrossRef]
51. Tawarmalani, M.; Sahinidis, N.V. *Convexification and Global Optimization in Continuous and Mixed-Integer Nonlinear Programming: Theory, Algorithms, Software, and Applications*; Kluwer Academic Publishers: New York, NY, USA, 2002; Volume 65.
52. Bonami, P.; Biegler, L.T.; Conn, A.R.; Cornuéjols, G.; Grossmann, I.E.; Laird, C.D.; Lee, J.; Lodi, A.; Margot, F.; Sawaya, N.; et al. An algorithmic framework for convex mixed integer nonlinear programs. *Discret. Optim.* **2008**, *5*, 186–204. [CrossRef]
53. Exler, O.; Lehmann, T.; Schittkowski, K. A comparative study of sqp-type algorithms for nonlinear and nonconvex mixed-integer optimization. *Math. Program. Comput.* **2012**, *4*, 383–412. [CrossRef]
54. Belotti, P.; Lee, J.; Liberti, L.; Margot, F.; Wächter, A. Branching and bounds tighteningtechniques for non-convex MINLP. *Optim. Methods Softw.* **2009**, *24*, 597–634. [CrossRef]
55. Bussieck, M.R.; Vigerske, S. *MINLP Solver Software*; GAMS Development Corp.: Merrifield, VA, USA, 2014.
56. Vazquez-Castillo, J.A.; Venegas-Sánchez, J.A.; Segovia-Hernández, J.G.; Hernández-Escoto, H.; Hernández, S.; Gutiérrez-Antonio, C.; Briones-Ramírez, A. Design and optimization, using genetic algorithms, of intensified distillation systems for a class of quaternary mixtures. *Comput. Chem. Eng.* **2009**, *33*, 1841–1850. [CrossRef]
57. Cheung, B.K.S.; Langevin, A.; Delmaire, H. Coupling genetic algorithm with a grid search method to solve mixed integer nonlinear programming problems. *Comput. Math. Appl.* **1997**, *34*, 13–23. [CrossRef]
58. Deb, K.; Pratap, A.; Agarwal, S.; Meyarivan, T. A fast and elitist multiobjective genetic algorithm: NSGA-II. *IEEE Trans. Evol. Comput.* **2002**, *6*, 182–197. [CrossRef]
59. Tayal, M.C.; Fu, Y.; Diwekar, U.M. Optimal design of heat exchangers: A genetic algorithm framework. *Ind. Eng. Chem. Res.* **1999**, *38*, 456–467. [CrossRef]
60. Kennedy, J.; Eberhart, R. Particle swarm optimization. In Proceedings of the ICNN'95—International Conference on Neural Networks, Perth, WA, Australia, 27 November–1 December 1995; Volume 4, pp. 1942–1948.
61. Glover, F. Tabu search part i. *ORSA J. Comput.* **1989**, *1*, 190–206. [CrossRef]
62. Dorigo, M. Optimization, Learning and Natural Algorithms. Ph.D. Thesis, Department of Electronics, Politecnico di Milano, Italy, 1992.

63. Schluter, M.; Gerdts, M. The oracle penalty method. *J. Glob. Optim.* **2010**, *47*, 293–325. [CrossRef]
64. Munawar, A.; Wahib, M.; Munetomo, M.; Akama, K. Advanced genetic algorithm to solve MINLP problems over gpu. In Proceedings of the 2011 IEEE Congress of Evolutionary Computation (CEC), New Orleans, LA, USA, 5–8 June 2011; pp. 318–325.
65. Gebreslassie, B.H.; Diwekar, U.M. Efficient ant colony optimization for computer aided molecular design: Case study solvent selection problem. *Comput. Chem. Eng.* **2015**, *78*, 1–9. [CrossRef]
66. Dong, M.; Cheng, X.; Niu, Q. A constrained particle swarm optimization algorithm with oracle penalty method. *Appl. Mech. Mater.* **2013**, *303–306*, 1519–1523. [CrossRef]
67. Schluter, M.; Egea, J.A.; Antelo, L.T.; Alonso, A.A.; Banga, J.R. An extended ant colony optimization algorithm for integrated process and control system design. *Ind. Eng. Chem. Res.* **2009**, *48*, 6723–6738. [CrossRef]
68. Schlüter, M. Nonlinear Mixed Integer Based Optimization Technique for Space Applications. Ph.D. Thesis, The University of Birmingham, Edgbaston, UK, 2012.
69. Schlüter, M.; Gerdts, M.; Rückmann, J.J. A numerical study of midaco on 100 minlp benchmarks. *Optimization* **2012**, *61*, 873–900. [CrossRef]
70. Sargent, R.W.H.; Westerberg, A.W. Speed-up in chemical engineering design. *Trans. Inst. Chem. Eng.* **1964**, 190–197. [CrossRef]
71. Tarjan, R. Depth-first search and linear graph algorithms. *SIAM J. Comput.* **1972**, *1*, 146–160. [CrossRef]
72. Motard, R.L.; Westerberg, A.W. Exclusive tear sets for flowsheets. *AIChE J.* **1981**, *27*, 725–732. [CrossRef]
73. Upadhye, R.S.; Grens, E.A. Selection of decompositions for chemical process simulation. *AIChE J.* **1975**, *21*, 136–143. [CrossRef]
74. Crespi, F.; Gavagnin, G.; Sánchez, D.; Martínez, G.S. Supercritical carbon dioxide cycles for power generation: A review. *Appl. Energy* **2017**, *195* (Suppl. C), 152–183.
75. Kumar, A.; Nakai, H.; Nakanishi, K.; Shimizu, H.; Hara, K.; Kojima, Y.; Honma, T. Design optimization of the 2 k heat exchanger for the superfluid helium cryogenic systems at kek. *Cryogenics* **2020**, *111*, 103173. [CrossRef]
76. Jin, F.; Yuan, D.; Chen, D.; Hu, L.; Huang, Y.; Bu, S. Experimental Study on Cooling Heat Transfer Performance of Supercritical CO_2 in Zigzag Printed Circuit Heat Exchanger. 2023, *preprint*. [CrossRef]
77. Jin, F.; Chen, D.; Hu, L.; Huang, Y.; Zeng, H.; Wang, J. Thermo-hydraulic performance of printed circuit heat exchanger as precooler in supercritical CO_2 brayton cycle. *Appl. Therm. Eng.* **2022**, *210*, 118341.
78. Stamatellos, G.; Stamatelos, T. Effect of actual recuperators' effectiveness on the attainable efficiency of supercritical CO_2 brayton cycles for solar thermal power plants. *Energies* **2022**, *15*, 7773. [CrossRef]
79. Wang, Z.; Xu, J.; Wang, T.; Miao, Z.; Wang, Q.; Liu, G. Performance of sCO_2 coal-fired power plants at various power capacities. *J. Clean. Prod.* **2023**, *416*, 137949. [CrossRef]
80. Zhao, Q. Conception and Optimization of Supercritical CO_2 Brayton Cycles for Coal-Fired Power Plant Application. Ph.D. Thesis, Lorraine University, Grand Est, France, 2018.
81. Feher, E.G. The supercritical thermodynamic power cycle Douglas Paper No.4348. In Proceedings of the Intersociety Energy Conversion Engineering Conference, Miami Beach, FL, USA, 13–17 August 1967; pp. 13–17.
82. Angelino, G. *Real Gas Effects in Carbon Dioxide Cycles*; ASME Paper, No. 69-GT-103:1–12; ASME: Little Falls, NJ, USA, 1969.